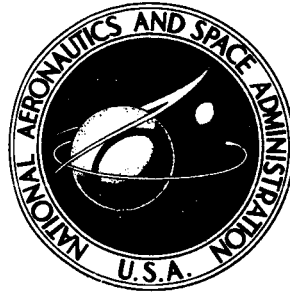


NASA TECHNICAL NOTE



N70-31624
NASA TN D-5796

NASA TN D-5796

CASE FILE COPY

HIGH-ALTITUDE FLIGHT TEST OF
A 40-FOOT-DIAMETER (12.2-METER)
RINGSAIL PARACHUTE AT A
DEPLOYMENT MACH NUMBER OF 2.95

by Clinton V. Eckstrom
Langley Research Center
Hampton, Va. 23365

NATIONAL AERONAUTICS AND SPACE ADMINISTRATION • WASHINGTON, D. C. • JUNE 1970

1. Report No. NASA TN D-5796	2. Government Accession No.	3. Recipient's Catalog No.	
4. Title and Subtitle HIGH-ALTITUDE FLIGHT TEST OF A 40-FOOT-DIAMETER (12.2-METER) RINGSAIL PARACHUTE AT A DEPLOYMENT MACH NUMBER OF 2.95		5. Report Date June 1970	
		6. Performing Organization Code	
7. Author(s) Clinton V. Eckstrom		8. Performing Organization Report No. L-7002	
		10. Work Unit No. 709-12-00-01	
9. Performing Organization Name and Address NASA Langley Research Center Hampton, Va. 23365		11. Contract or Grant No.	
		13. Type of Report and Period Covered Technical Note	
12. Sponsoring Agency Name and Address National Aeronautics and Space Administration Washington, D.C. 20546		14. Sponsoring Agency Code	
		15. Supplementary Notes Technical Film Supplement L-1077 available on request.	
16. Abstract <p>A 40-foot-nominal-diameter (12.2-meter) modified ringsail parachute was flight tested as part of the NASA Supersonic High Altitude Parachute Experiment (SHAPE) program. The 41-pound (18.6-kg) test parachute system was deployed from a 239.5-pound (108.6-kg) instrumented payload by means of a deployment mortar when the payload was at a Mach number of 2.95 and a free-stream dynamic pressure of 9.2 lb/sq ft (440 N/m²). The parachute deployed properly with the canopy inflating to a near full open condition followed immediately by a partial collapse of the canopy and subsequent oscillations of the frontal area until the system had decelerated to a Mach number of about 1.5. The parachute then attained an inflated shape that provided full drag area. During the supersonic part of the test, the average axial-force coefficient $C_{A,0}$ varied from a minimum of about 0.24 at a Mach number of 2.7 to a maximum of 0.54 at a Mach number of 1.1. During descent under subsonic conditions, the average effective drag coefficient was 0.62 and parachute-payload oscillation angles averaged about $\pm 10^\circ$ with excursions to $\pm 20^\circ$.</p>			
17. Key Words (Suggested by Author(s)) Ringsail parachutes Parachute flight tests Decelerator		18. Distribution Statement Unclassified - Unlimited	
19. Security Classif. (of this report) Unclassified	20. Security Classif. (of this page) Unclassified	21. No. of Pages 49	22. Price* \$3.00

HIGH-ALTITUDE FLIGHT TEST OF A
40-FOOT-DIAMETER (12.2-METER) RINGSAIL PARACHUTE
AT A DEPLOYMENT MACH NUMBER OF 2.95

By Clinton V. Eckstrom
Langley Research Center

SUMMARY

A 40-foot-nominal-diameter (12.2-meter) modified ringsail parachute was flight tested as part of the NASA Supersonic High Altitude Parachute Experiment (SHAPE) program. The 41-pound (18.6-kg) test parachute system was deployed from a 239.5-pound (108.6-kg) instrumented payload by means of a deployment mortar when the payload was at an altitude of 171 400 feet (52.3 km), a Mach number of 2.95, and a free-stream dynamic pressure of 9.2 lb/sq ft (440 N/m²). The parachute deployed properly, suspension line stretch occurring 0.54 second after mortar firing with a resulting snatch-force loading of 932 pounds (4146 newtons). The maximum loading due to parachute opening was 5162 pounds (22 962 newtons) at 1.29 seconds after mortar firing. The first near full inflation of the canopy at 1.25 seconds after mortar firing was followed immediately by a partial collapse and subsequent oscillations of frontal area until the system had decelerated to a Mach number of about 1.5. The parachute then attained a shape that provided full drag area. During the supersonic part of the test, the average axial-force coefficient $C_{A,0}$ varied from a minimum of about 0.24 at a Mach number of 2.7 to a maximum of 0.54 at a Mach number of 1.1. During descent under subsonic conditions, the average effective drag coefficient was 0.62 and parachute-payload oscillation angles averaged about $\pm 10^\circ$ with excursions to $\pm 20^\circ$. The recovered parachute was found to have slight damage in the vent area caused by the attached deployment bag and mortar lid.

INTRODUCTION

The NASA SHAPE Program is a continuation of earlier efforts to provide data on the performance of parachutes in low-density environments. (See refs. 1, 2, and 3.) The SHAPE Program was aimed at higher Mach number deployments than had previously been accomplished at relatively low dynamic pressures.

This report presents data from the flight test of a 40-foot-nominal-diameter (12.2-meter) modified ringsail parachute deployed at a Mach number of 2.95. The test parachute had the same number of panels per gore (rings and sails) and a porosity

distribution similar to a larger (54.5-foot-nominal-diameter (16.6-meter)) modified ringsail parachute which had previously been deployed at a Mach number of 1.6 and a dynamic pressure of 11.6 lb/sq ft (555 N/m²) as reported in reference 4. Other modified ringsail parachutes having variations in the number of ring and/or sail panels per gore, variations in the distribution of geometric porosity, and/or significantly different cloth permeability have been flight tested as reported in reference 3. The 54.5-foot (16.6-meter) modified ringsail parachute exhibited the best performance of the previously tested ringsail parachutes, and therefore the primary purpose of this flight test was to determine the performance of a similar ringsail parachute at a significantly increased Mach number. In addition, this test was the second high-altitude flight test where the parachute deployment bag and mortar lid remained attached to the apex of the parachute canopy after deployment to eliminate possible canopy damage due to collision with the free flying bag and lid combination.

Motion-picture film supplement L-1077 is available on loan; a request card and a description of the film are included at the back of this paper.

SYMBOLS

a_x	acceleration along longitudinal axis of payload, g units
$C_{A,o}$	nominal axial-force coefficient
$C_{D,o}$	drag coefficient, average of calculated $C_{A,o}$ values
$(C_{D,o})_{\text{eff}}$	effective drag coefficient (based on vertical descent velocity and acceleration)
D_o	nominal diameter, $\left(\frac{4S_o}{\pi}\right)^{1/2}$, ft (m)
g	acceleration due to gravity, 32.2 ft/sec ² (9.81 m/sec ²)
M	Mach number
m	mass, slugs (kg)
Δp	differential pressure, in. H ₂ O (cm H ₂ O)
q_∞	free-stream dynamic pressure, $\frac{1}{2}\rho_\infty V^2$, lb/ft ² (N/m ²)
S_o	nominal surface area of parachute canopy including gap and vent, ft ² (m ²)

S_p	projected area of parachute canopy, ft ² (m ²)
t	time from vehicle liftoff, sec
t'	time from mortar firing, sec
V	true airspeed, ft/sec (m/sec)
X, Y, Z	payload body-axis system
X_f, Y_f, Z_f	earth-fixed axis system
Z_E	local vertical axis, positive down
δ_E	payload resultant pitch-yaw angle from local vertical, deg
θ, ψ, ϕ	gyro platform angles relating body-axis system to inertial coordinate system (gyro-uncaging position), deg
θ_E, ψ_E, ϕ_E	Euler angles relating body-axis system to earth-fixed axis system, deg
ρ	atmospheric density, slugs/ft ³ (kg/m ³)

Subscripts:

av	average
eff	effective
max	maximum
meas	measured
std	standard
∞	free stream

Dots over symbols denote differentiation with respect to time.

TEST SYSTEM

The instrumented payload was carried to the test point by means of an Honest John-Nike-Nike rocket vehicle. A photograph of the test vehicle in the launch position is presented as figure 1. A sketch of the test payload (fig. 2) locates primary components and

the onboard instrumentation. The payload and test instrumentation have been described in reference 5. The test parachute was deployed from the payload by the large mortar. This payload mortar system consisting of the tube, breach, cartridges, and sabot, but excluding the batteries, weighed 17.25 pounds (7.8 kg). The mortar cover weight of 1 pound (0.45 kg) is considered as part of the parachute system weight. The suspended payload weight including the mortar system and the attachment bridle and tensiometer was 239.5 pounds (108.6 kg) and the parachute system weight was 41.0 pounds (18.6 kg) for a total descent weight of the payload-parachute system of 280.5 pounds (127.2 kg).

TEST PARACHUTE

The test parachute was a modified ringsail design having a nominal diameter D_0 of 40 feet (12.2 meters), a reference area S_0 of 1256 sq ft (116.7 m²), and suspension lines which were 48 feet (14.6 meters) or $1.2D_0$ long. Figure 3 presents the layout of a gore and the general parachute-payload configuration. The parachute canopy consisted of 36 gores, each gore having 10 panels – the upper four of which were separated by slots and are referred to as rings. The lower panels had fullness at their bottom edges to provide geometric porosity and these panels are referred to as sails. The removal of a sail in the lower portion of the gore to provide the desired total geometric porosity was the major modification to the standard ringsail design. The vent area at the apex of the canopy provided 0.5-percent open area and the slots between the rings provided another 0.7-percent open area for a total crown geometric porosity of 1.2 percent. The omitted sail provided 9.7-percent open area and the scoops formed by the sail panels contributed another 3.9 percent for a total geometric porosity of 14.8 percent of the total surface or reference area S_0 . A complete listing of gore dimensions is provided in table I.

The gore panels of the test parachute were fabricated from material woven in a rip-stop pattern but also having a 1.5-inch (3.8-cm) reinforced selvage edge along both the top and bottom edge. The total woven material width including the selvage edges was 24.5 inches (62.2 cm). For some sails, the upper selvage edge was folded over and sewn to give the proper panel height of $23\frac{3}{4}$ inches (60.33 cm). The material was woven from 55 denier high-tenacity type 52 dacron with a selvage edge strength of 182.6 pounds (812.2 newtons) and a fabric strength of 69 lb/in. (120.8 N/cm) in both the warp and fill direction. This canopy cloth was woven specifically for this test parachute to provide the proper material width and the desired edge strength. The canopy radial and circumferential reinforcement and structural tapes and the parachute suspension lines were also woven of high-tenacity type 52 dacron but were similar to tapes and lines used on previous flight-test parachutes. The parachute characteristics and material properties are presented in table II and the component weights of the payload-parachute system are presented in table III.

The parachute was packed in a split cylindrical deployment bag of dacron canvas (lined with teflon cloth) as shown in figure 4. The parachute deployment bag and mortar lid combination were permanently attached to the canopy apex by 9 lines, each 50 inches (127 cm) long, which ran from the canopy vent edge to the inside of the bag and attached at the base of the bag to both the bag and the mortar lid. Figure 5 shows the mortar lid and bag attached to the parachute after the flight test was completed and the parachute was laid out for on-site inspection.

TABLE I.- DETAIL GORE DIMENSIONS

Item	Panel width				Vertical height	
	Top		Bottom		in.	cm
	in.	cm	in.	cm		
Vent	0	0	$3\frac{13}{32}$	8.65	$18\frac{7}{32}$	46.28
Ring 1	$3\frac{13}{32}$	8.65	$7\frac{11}{32}$	18.65	$23\frac{3}{4}$	60.33
Slot 1	$7\frac{11}{32}$	18.65	$7\frac{17}{32}$	19.13	$1\frac{1}{8}$	2.86
Ring 2	$7\frac{17}{32}$	19.13	$11\frac{7}{16}$	29.05	$23\frac{3}{4}$	60.33
Slot 2	$11\frac{7}{16}$	29.05	$11\frac{9}{16}$	29.37	$\frac{13}{16}$	2.06
Ring 3	$11\frac{9}{16}$	29.37	$15\frac{15}{32}$	39.29	$24\frac{1}{2}$	62.23
Slot 3	$15\frac{15}{32}$	39.29	$15\frac{9}{16}$	39.53	$\frac{5}{8}$	1.59
Ring 4	$15\frac{9}{16}$	39.53	$19\frac{11}{32}$	49.13	$24\frac{1}{2}$	62.23
Slot 4	$19\frac{11}{32}$	49.13	$19\frac{7}{16}$	49.37	$\frac{1}{2}$	1.27
Sail 5	$19\frac{7}{16}$	49.37	$23\frac{7}{16}$	59.53	$23\frac{3}{4}$	60.33
Sail 6	$22\frac{3}{4}$	57.79	$27\frac{3}{32}$	68.82	$23\frac{3}{4}$	60.33
Sail 7	$25\frac{15}{16}$	65.88	$30\frac{19}{32}$	77.71	$23\frac{3}{4}$	60.33
Missing sail					$16\frac{9}{16}$	42.07
Sail 9	$31\frac{1}{16}$	78.90	$36\frac{5}{32}$	91.84	$23\frac{3}{4}$	60.33
Sail 10	$33\frac{25}{32}$	85.80	$39\frac{7}{32}$	99.62	$24\frac{1}{2}$	62.23

TABLE II.- PARACHUTE CHARACTERISTICS AND MATERIAL PROPERTIES

Parachute type	Modified ringsail
Nominal diameter, D_0 , ft (m)	40 (12.2)
Nominal area, S_0 , ft ² (m ²)	1256 (116.7)
Number of gores and suspension lines	36
Length of suspension lines ($1.2D_0$), ft (m)	48 (14.6)
Geometric porosity (total canopy), percent	14.8
Crown porosity, percent	1.2
Canopy cloth (rip-stop pattern):	
Unit weight (including selvage edge), oz/sq yd (g/m ²)	1.53 (51.9)
Maximum elongation (average of five measurements), percent -	
Filling	39.5
Warp	31.5
Tensile strength (ravel strip method) (average of five measure- ments) (both warp and filling directions), lb/in. (N/cm)	69.0 (120.8)
Permeability (average at 0.5 in. H ₂ O (1.27 cm H ₂ O) Δp ; average of five measurements), ft ³ /min/ft ² (m ³ /min/m ²)	160 (48.8)
Tear strength (tongue tear method) (average of five measurements), lb (N)	7.1 (31.6)
Radial and circumferential tapes:	
Width, in. (cm)	3/4 (1.9)
Thickness, in. (cm)	0.027 (0.069)
Unit weight, oz/yd (g/m)	0.277 (7.18)
Maximum elongation (measured), percent	28
Tensile strength (measured), lb (N)	582 (2589)
Suspension lines, coreless braided:	
Unit weight, oz/yd (g/m)	0.268 (6.95)
Maximum elongation, percent	44
Tensile strength (minimum measured), lb (N)	590 (2.624)
Riser webbing, low elongation (MIL-W-25361A):	
Width, in. (cm)	$1\frac{23}{32}$ (4.37)
Thickness, in. (cm)	0.082 (0.208)
Unit weight, oz/yd (g/m)	2.29 (59.4)
Elongation at 90 percent of ultimate (measured), percent	13
Tensile strength (minimum of five measurements), lb (N)	8720 (38 788)

TABLE III.- PARACHUTE-PAYLOAD SYSTEM WEIGHT BREAKDOWN

	lb	kg
Mortar lid weight	1.0	0.45
Parachute deployment bag weight	0.9	0.41
Parachute weight including canopy lines, and upper riser	35.3	16.00
	lb	kg
Canopy cloth (calculated)	14.1	6.40
Radial tapes (calculated)	5.1	2.31
Circumferential tapes (calculated)	3.0	1.36
Thread and ink (calculated)	1.7	0.76
Suspension lines (calculated)	9.8	4.45
Upper riser (calculated)	1.6	0.72
Swivel and fitting	2.5	1.13
Intermediate riser and fittings	1.3	0.59
Tensiometer	1.5	0.68
Bridle	1.5	0.68
Payload	<u>236.5</u>	<u>107.27</u>
Total system weight	280.5	127.21

RESULTS AND DISCUSSION

Test Data

The flight-test vehicle was launched at 10:17 a.m., mdt, on June 18, 1969, at White Sands Missile Range, New Mexico. Figure 6 presents the flight sequence and the recorded times for significant flight events. Time histories of payload altitude and relative velocity for the first 360 seconds of the flight as measured by FPS-16 radar are shown in figure 7.

Meteorological data used in analysis of the parachute test data were provided by means of an ARCAS meteorological sounding rocket launched 2 hours and 43 minutes after the flight test. These data were supplemented by data from a rawinsonde which was released 4 hours and 17 minutes before the flight-test vehicle was launched. The atmospheric density derived from measured temperature profiles expressed as a ratio to the 1962 U.S. Standard Atmosphere values (ref. 6) is presented in figure 8 and upper altitude winds as determined from the rocket sounding are presented in figure 9. The estimated uncertainty of the derived density ranges from ± 3 percent from ground level to about

150 000 feet (46 km) altitude increasing to about ± 8 percent at 200 000 feet (61 km). The estimated uncertainty of the upper altitude winds presented in figure 9 range from ± 5 percent at 100 000 feet (30 km) to ± 20 percent at 200 000 feet (61 km).

Telemetered accelerometer data and radar track data were used to determine histories of payload true airspeed and Mach number which are presented in figure 10. By definition, the initiation of parachute deployment corresponds to mortar firing ($t' = 0$). The derived atmospheric density data were used with the payload true airspeed to determine the dynamic pressure during the test period which is shown in figure 11. Parachute deployment was initiated at a velocity of 3137 ft/sec (956 m/sec) or $M = 2.95$, a dynamic pressure of 9.2 lb/sq ft (440 N/m²), and an altitude of 171 400 feet (52.3 km) above mean sea level. The estimated uncertainty of the deployment conditions based on a ± 2 -percent velocity error, ± 3 -percent temperature error, and ± 5 -percent density error are ± 0.11 for the Mach number and ± 0.5 lb/sq ft (± 22 N/m²) for the dynamic pressure by using a first-order error analysis.

The history of force transmitted through the riser line as measured by the tensiometer during the primary test period is presented in figure 12. The first peak load of 920 pounds (4092 newtons) at $t' = 0.33$ second is attributed to the full-length deployment of the parachute riser system. The second peak force of 932 pounds (4146 newtons) at $t' = 0.54$ second was the snatch force encountered when the suspension lines were fully extended and canopy deployment began. The largest peak force of 5162 pounds (22 962 newtons) at $t' = 1.29$ seconds occurred immediately (0.04 second) after the parachute reached the maximum frontal area (first inflation) in the opening process. During the canopy inflation process, which began immediately after line stretch at $t' = 0.54$ second and ended at $t' = 1.25$ seconds, the force measured by the tensiometer decreased from 2810 pounds (12 500 newtons) at $t' = 1.18$ seconds to about 400 pounds (1780 newtons) at $t' = 1.22$ seconds and then increased to the maximum opening load at $t' = 1.29$ seconds as was mentioned earlier. This type of load variation at initial inflation, which also continued for several seconds at a frequency of about 8 cycles per second, is believed to be a result of the oscillations set up by the elastic suspension lines and is the most probable reason that the maximum frontal area and the peak opening load did not occur at the exact same time. This phenomenon has been encountered on previous flight tests (refs. 7 and 8), and an analytical simulation was presented as an appendix to reference 7. The estimated uncertainty of the recorded tensiometer data is ± 50 pounds (220 newtons).

Figure 13 presents the data from three accelerometers located in the payload as measured for the first 20 seconds after mortar firing. Deceleration loads calculated from measured longitudinal accelerometer data are in close agreement with those recorded by the tensiometer.

Pitch and yaw motions recorded by the gyro platform during the first 14 seconds after mortar firing are shown in figure 14. Pitch angle θ and yaw angle ψ at $t' = 0$ are the direct measurements from the gyro platform referenced to the gyro offset angles introduced prior to vehicle lift-off. The gyro offset procedure was performed to counter the effects of high-altitude winds expected at flight apogee and thereby prevent the gyro platform from exceeding its yaw operating limits which would result in a loss of data for the remainder of the flight. The gyro platform offset procedure is discussed in detail in reference 9. The gyro platform pitch and yaw data presented give a good measure of motions of the payload resulting from the varying loads imparted to the payload during the parachute deployment and inflation period and during the period of large-amplitude variations in loads transmitted to the payload through the parachute attachment system. The payload angular rates for this flight test were relatively high with an angular rate of over 400° per second occurring at about $t' = 2.6$ seconds. The estimated uncertainty of the gyro data is $\pm 2^\circ$ for all three axes.

The roll angle ϕ of the payload as measured by the gyro platform and the roll angle of the parachute relative to earth-fixed axes as determined from the aft camera film are presented in figure 15 for the first 20 seconds after mortar firing. The estimated uncertainty of the parachute roll angle is $\pm 5^\circ$. The flight system was not spin stabilized; however, the payload had attained a roll rate of about 1 revolution per second at mortar fire. Shortly after the parachute opened, the roll rate of the payload decreased and steadied to about 0.17 revolution per second during the period from $t' = 4.0$ seconds to $t' = 20$ seconds as shown in figure 15. The roll-angle measurements on the parachute were referenced to its position at $t' = 1.17$ seconds when the canopy markings were first clearly visible. Initially, the parachute had little or no roll but after about $t' = 4.0$ seconds, the parachute began to roll slowly in the same direction as the payload; however, it attained less than 1 revolution during the 20-second data period. A swivel in the riser system allowed different roll rates for the payload and the parachute.

Analysis of Parachute Performance

Deployment.- The test parachute was mortar deployed from the payload at an average ejection velocity of 115 ft/sec (35.0 m/sec) based on a total suspension line plus attachment system length of 62 feet (18.8 meters) (parachute suspension lines were 48 feet (14.6 meters) or $1.2D_0$ long) and a measured time to line stretch of 0.54 second. As mentioned previously, the resulting snatch force was 932 pounds (4146 newtons).

Canopy inflation.- Figure 16 presents selected frames from the aft camera film showing the initial canopy inflation, the collapse sequence, the load-variation sequence, inflation-stabilization sequence, and the canopy operating in the full-open condition.

The parachute projected-area ratio is presented in the upper part of figure 17. Note that the first inflation of the canopy occurred in a normal manner with the projected area increasing smoothly from the time of line stretch to about 85-percent full open at $t' = 1.25$ seconds. Immediately thereafter, the frontal area decreased again and fluctuated from about 40 to 90 percent full open until 12.25 seconds after mortar firing or until the system velocity decreased to less than Mach 1.5. The final parachute frontal area $S_{p,final}$ was determined after the system attained subsonic velocity as shown in figure 16(e).

Drag efficiency.- The axial-force coefficient $C_{A,o}$ is also presented in figure 17 as a function of time from mortar deployment. In addition to the time scale, a Mach number scale is shown for reference. The axial-force coefficient shown was determined from accelerometer data based on the following equation:

$$C_{A,o} = - \frac{m_{total} g a_x}{q_{\infty} S_o}$$

(Since payload drag was very small compared with parachute drag, it was neglected in the calculations.) The estimated uncertainty in $C_{A,o}$ varied from ± 0.04 at parachute deployment to ± 0.07 at the end of 20-second supersonic data period. This range of uncertainty is based on a first-order error analysis using an estimated inaccuracy of the derived density ranging from ± 5 percent at parachute deployment to ± 8 percent at the end of the data period, a true airspeed error ranging from ± 2 percent at parachute deployment to ± 5 percent at the end of the data period and an accelerometer error ranging from ± 2.5 percent at parachute deployment to ± 5 percent at the end of the data period. For the first 12.25 seconds of operation during which the flight Mach number was greater than 1.5, the axial-force coefficient $C_{A,o}$ varied from 0.8 to near zero. At the lower Mach number range ($1.5 > M > 1.0$), the axial-force-coefficient variation was significantly less. The large variations in axial-force coefficient $C_{A,o}$ at Mach numbers greater than 1.5 reflect the large variations found in the longitudinal accelerometer history of figure 13 and are believed to be the effect of oscillations in the elastic suspension-line system initiated by the opening loads and sustained by the continuously varying drag-producing area of the parachute canopy at Mach numbers greater than 1.5 as shown by the upper part of figure 17. The effect of the cyclic variation of parachute frontal area is evident in the variation of the axial-force coefficient. As an example, from $t' = 7.0$ seconds to $t' = 7.75$ seconds, the parachute frontal area goes from 41 percent of full open area to 85 percent and back to a minimum value of 44 percent. During this same time period, the axial-force coefficient follows the same trend as the parachute frontal area variation with the addition of a higher frequency variation superimposed. A mathematical model contained in an appendix to reference 7 effectively simulates a similar oscillatory load history when the varying drag-producing area is used as an input to the calculations. As

the system decelerated to velocities less than Mach 1.5, the parachute attained a more stable shape that resulted in smaller variations in the axial-force-coefficient data as shown in the lower part of figure 17. A review of the aft camera film indicated that at velocities less than Mach 1.5, the part of the ringsail canopy above the missing sail had essentially attained inflation stability whereas the two sails below the missing sail continued to fluctuate from an underinflated condition to substantial overinflation as evidenced by the oscillation near the value $\frac{S_p}{S_{p,final}} = 1.0$ on the upper part of figure 17. However, this fluctuation of the lower two sails did not seem to affect significantly the load history as shown by figures 12 and 13 or the axial-force coefficient as shown in the lower part of figure 17.

The variation of the vertical descent velocity and the effective drag coefficient are presented in figure 18. The values of effective drag coefficient are based on vertical descent velocity and acceleration and the system mass as shown by the following equation:

$$(C_{D,o})_{eff} = \frac{2m_{total}}{\rho_{\infty} \dot{z}_E^2 S_o} (g - \ddot{z}_E)$$

During the descent portion of the flight test from 160 000 feet (48.8 km) to 48 000 feet (14.6 km), the average effective drag coefficient $(C_{D,o})_{eff}$ was about 0.62. The estimated uncertainty of $(C_{D,o})_{eff}$ is ± 0.05 based on a first-order error analysis and estimated uncertainties of ± 3 percent in density and ± 5 percent in vertical velocity.

Average values of axial-force coefficient $C_{A,o}$ were determined at every 0.1 Mach number over the established data period and these average values are presented in figure 19 as drag coefficient $C_{D,o}$ as a function of Mach number. During the supersonic part of the flight test, the average axial-force coefficient varied from a minimum of about 0.24 at a Mach number of 2.7 to a maximum of 0.54 at a Mach number of 1.1. These data are essentially the same as those presented in figure 17 with the exception that more data points were used in establishing average values than were plotted in figure 17. In addition, average values of $(C_{D,o})_{eff}$ from figure 18 are presented to complete the lower Mach number part of the figure.

The reduction in drag coefficient $C_{D,o}$ at the higher Mach numbers is due partially to the reduced parachute frontal area. In an attempt to show the possible correlation, the frontal area data shown in figure 17 was averaged over the same Mach number intervals as the $C_{D,o}$ data. Note that above Mach 1.7, there are several discontinuities in the frontal area data which affect the averages shown. This average frontal area data is shown in figure 20 along with the $C_{D,o}$ values expressed as a ratio to the $C_{D,o}$ value of 0.545 occurring at $M = 1.1$. It is evident from figure 20 that a large part of the reduced drag efficiency at the higher Mach numbers is directly attributable to the reduced frontal area.

Stability.- The payload pitch and yaw motions and the payload and parachute roll rates immediately after parachute deployment were discussed earlier with data presented in figures 14 and 15.

During the descent portion of the flight test (from an altitude of 136 500 feet (41.6 km) down to an altitude of 109 500 feet (33.4 km)), the gyro platform data were transformed to the earth-fixed Euler angle system shown in figure 21 by the method presented in an appendix to reference 9. The resulting data are presented in figure 22. Although the aft camera film did not cover this data period, results from a previous flight test (ref. 10) lead to the expectation that the data shown in figure 22 should represent the attitude history of the payload and parachute acting together like a rigid body and should therefore be a direct indication of the stability of the test parachute. As can be seen from figure 22, the average payload position in the pitch plane is slightly positive (8.7°) and the average payload position in the yaw plane is slightly negative (-5.0°). The payload resultant angle $|\delta_E|$ was determined relative to the average position in the pitch and yaw planes and, as shown in figure 22, was generally less than 10° with occasional excursions to near 20° . A photograph of the descending parachute and payload is presented in figure 23. The modified ringsail parachute was an effective decelerator over the entire flight-test altitude range from about 220 000 feet (67 km) to ground level.

Parachute inspection.- A postflight inspection of the recovered parachute located specific damaged areas as shown in figures 24 and 25. All the damage found was minor and no adverse effect on the performance of the parachute was noted. The damage in the vent area is attributed to impact with the parachute deployment bag and mortar lid which were attached to the parachute canopy in the vent area. All the damage in the vent area occurred immediately after deployment. It was determined from the aft camera film that the bag and lid penetrated the parachute canopy (panel 1, gore 34) at $t' = 4.75$ seconds and remained on the interior of the canopy for the remainder of the flight. A total of 12 panels in the vent area were damaged. There were seven panels in ring 1 damaged with the damage ranging from a 0.5-inch-diameter (1.3-cm) hole in gore 22 to full-length panel damage in gore 34. There were 3 panels damaged in ring 2. In ring 3, the panel in gore 11 had a small hole, about 0.75-inch (1.9-cm) diameter and in ring 4, the panel in gore 5 had a small slit about 0.75 inch (1.9 cm) long. In addition, there were three sail panels damaged in ring 10. Sails 10 in gores 28 and 29 were torn at the radial tape as shown in figure 26 and sail 10 in gore 32 had 5 small holes about 0.5-inch (1.3-cm) diameter.

At each point marked with a circle in figure 24, the top edge of one panel and the bottom edge of the adjacent panel were pulled from the radial tape for lengths of from 0.5 inch (1.3 cm) to 3 inches (7.6 cm) at these joints. These failures were stitching

failures with no damage to the canopy radial tapes or cloth which probably resulted from sail flutter during the high Mach number part of the flight test.

In addition to the damage analysis, there were several measurements taken during the postflight inspection. Each of the suspension lines were measured (with 20 pounds (89 newtons) tension) and found to be from 1 to 7 inches (2.5 to 17.8 cm) longer than before the flight test. This slight change in length represents an increase of only 0.2 to 1.2 percent of the original length. Radial tapes number 1, 21, and 36 were measured, radial tape 1 being 2.25 inches (5.7 cm) longer, radial tape 21 being 1.25 inches (3.2 cm) longer, and radial tape 36 having no change from preflight measurements. The top and bottom width of each panel in gore 36 were measured before and after the flight test, no noticeable changes being detected.

CONCLUSIONS

The 40-foot-nominal-diameter (12.2-meter) modified ringsail test parachute having 48-foot-long (14.6-meter) suspension lines was deployed from an instrumented payload by means of a deployment mortar when the payload was at a Mach number of 2.95 and a free-stream dynamic pressure of 9.2 lb/sq ft (440 N/m²). Based on an analysis of the data, it is concluded that:

1. The mortar properly ejected the parachute system from the payload.
2. The parachute deployed properly with the canopy inflating to about 85 percent of the full open condition at 1.25 seconds after mortar firing. The parachute then assumed a fluctuating partially inflated shape until the system had decelerated to a Mach number of about 1.5 at which time the parachute attained an inflated shape essentially providing full drag area.
3. During the supersonic part of the flight test, the average axial-force coefficient varied from a minimum of about 0.24 at a Mach number of 2.7 to a maximum of 0.54 at a Mach number of 1.1.
4. During descent under subsonic conditions, the average effective drag coefficient was 0.62 and the parachute-payload oscillation angles averaged about $\pm 10^\circ$ with excursions to $\pm 20^\circ$.
5. The maximum load due to parachute opening was 5162 pounds (22 962 newtons) at 1.29 seconds after mortar firing.
6. The parachute was subjected to minor damage in several areas but primarily in the vent area where the deployment-bag—mortar-lid combination was attached to the canopy. It is believed that the damage sustained did not affect the performance of the parachute.

7. The modified ringsail parachute was an effective decelerator over the entire flight-test altitude range from about 220 000 feet (67 km) to ground level.

Langley Research Center,
National Aeronautics and Space Administration,
Hampton, Va., April 17, 1970.

REFERENCES

1. McFall, John C., Jr.; and Murrow, Harold N.: Parachute Testing at Altitudes Between 30 and 90 Kilometers. *J. Spacecraft Rockets (Eng. Notes)*, vol. 4, no. 6, June 1967, pp. 796-798.
2. Murrow, Harold N.; and McFall, John C., Jr.: Some Test Results From the NASA Planetary Entry Parachute Program. *J. Spacecraft Rockets (Eng. Notes)*, vol. 6, no. 5, May 1969, pp. 621-623.
3. Whitlock, Charles H.; and Bendura, Richard J.: Inflation and Performance of Three Parachute Configurations From Supersonic Flight Tests in a Low-Density Environment. NASA TN D-5296, 1969.
4. Whitlock, Charles H.; Henning, Allen B.; and Coltrane, Lucille C.: Performance of a 16.6-Meter-Diameter Modified Ringsail Parachute in a Simulated Martian Environment. NASA TM X-1500, 1968.
5. Preisser, John S.; Eckstrom, Clinton V.; and Murrow, Harold N.: Flight Test of a 31.2-Foot-Diameter Modified Ringsail Parachute Deployed at a Mach Number of 1.39 and a Dynamic Pressure of 11.0 Pounds Per Square Foot. NASA TM X-1414, 1967.
6. Anon.: U.S. Standard Atmosphere, 1962. NASA, U.S. Air Force, and U.S. Weather Bur., Dec. 1962.
7. Eckstrom, Clinton V.; and Preisser, John S.: Flight Test of a 40-Foot-Nominal-Diameter Disk-Gap-Band Parachute Deployed at a Mach Number of 2.72 and a Dynamic Pressure of 9.7 Pounds Per Square Foot. NASA TM X-1623, 1968.
8. Eckstrom, Clinton V.: Flight Test of a 40-Foot-Nominal-Diameter Disk-Gap-Band Parachute Deployed at a Mach Number of 3.31 and a Dynamic Pressure of 10.6 Pounds Per Square Foot. NASA TM X-1924, 1970.
9. Preisser, John S.; and Eckstrom, Clinton V.: Flight Test of a 30-Foot-Nominal-Diameter Cross Parachute Deployed at a Mach Number of 1.57 and a Dynamic Pressure of 9.7 Pounds Per Square Foot. NASA TM X-1542, 1968.
10. Preisser, John S.; and Eckstrom, Clinton V.: Flight Test of a 40-Foot-Nominal-Diameter Disk-Gap-Band Parachute Deployed at a Mach Number of 1.91 and a Dynamic Pressure of 11.6 Pounds Per Square Foot. NASA TM X-1575, 1968.

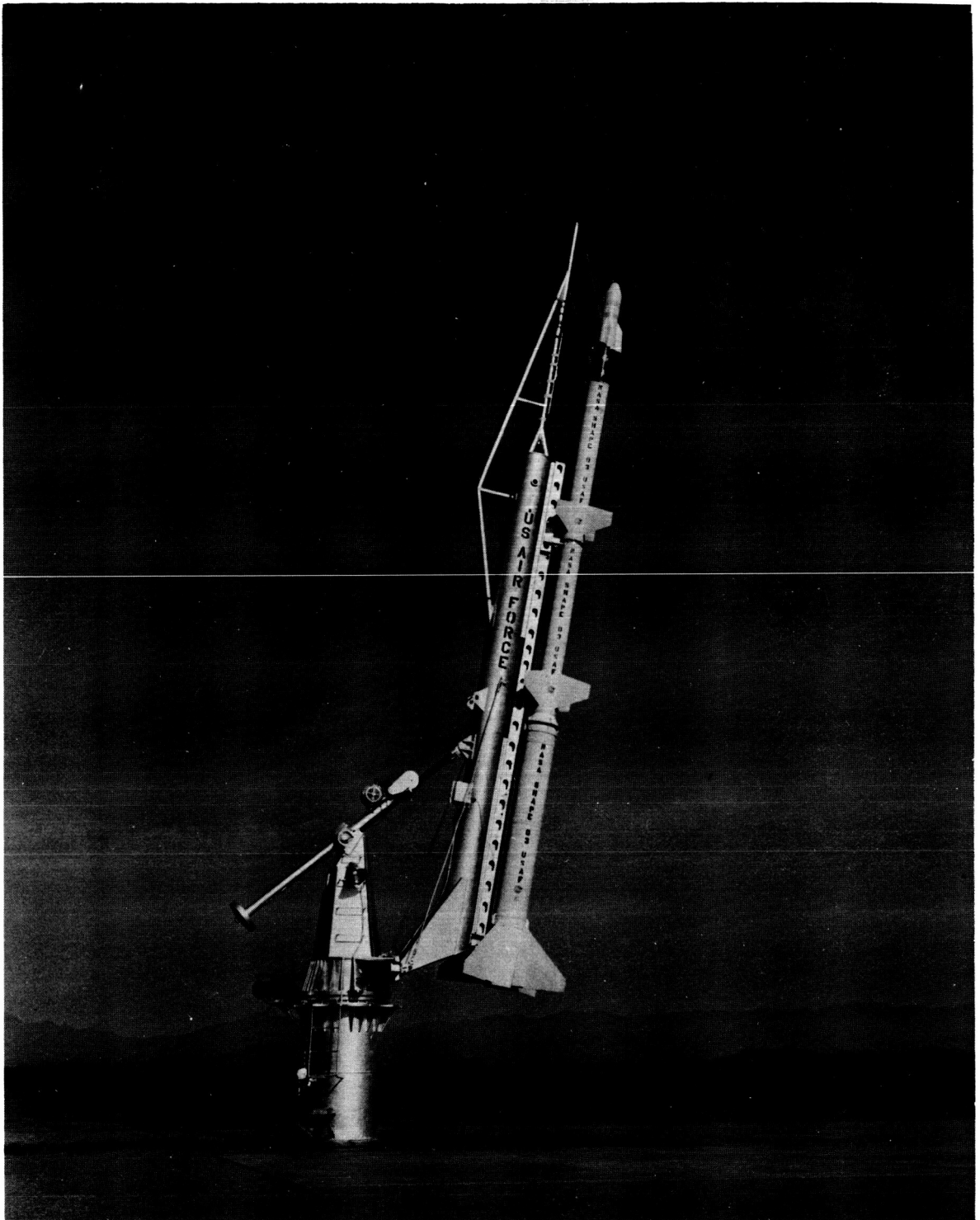


Figure 1.- Vehicle configuration. U.S. Army photograph.

L-70-1589

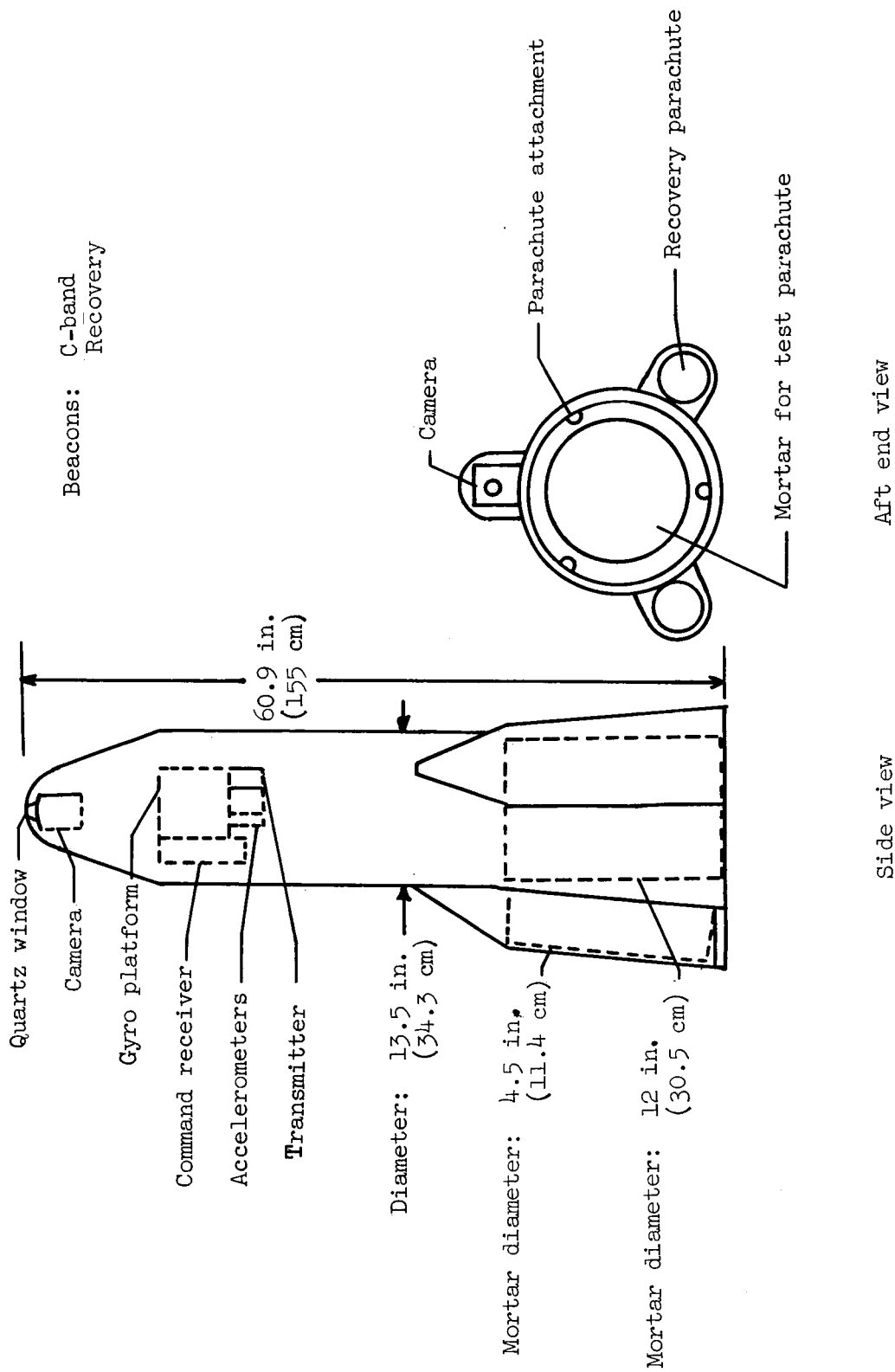


Figure 2.- Test payload.

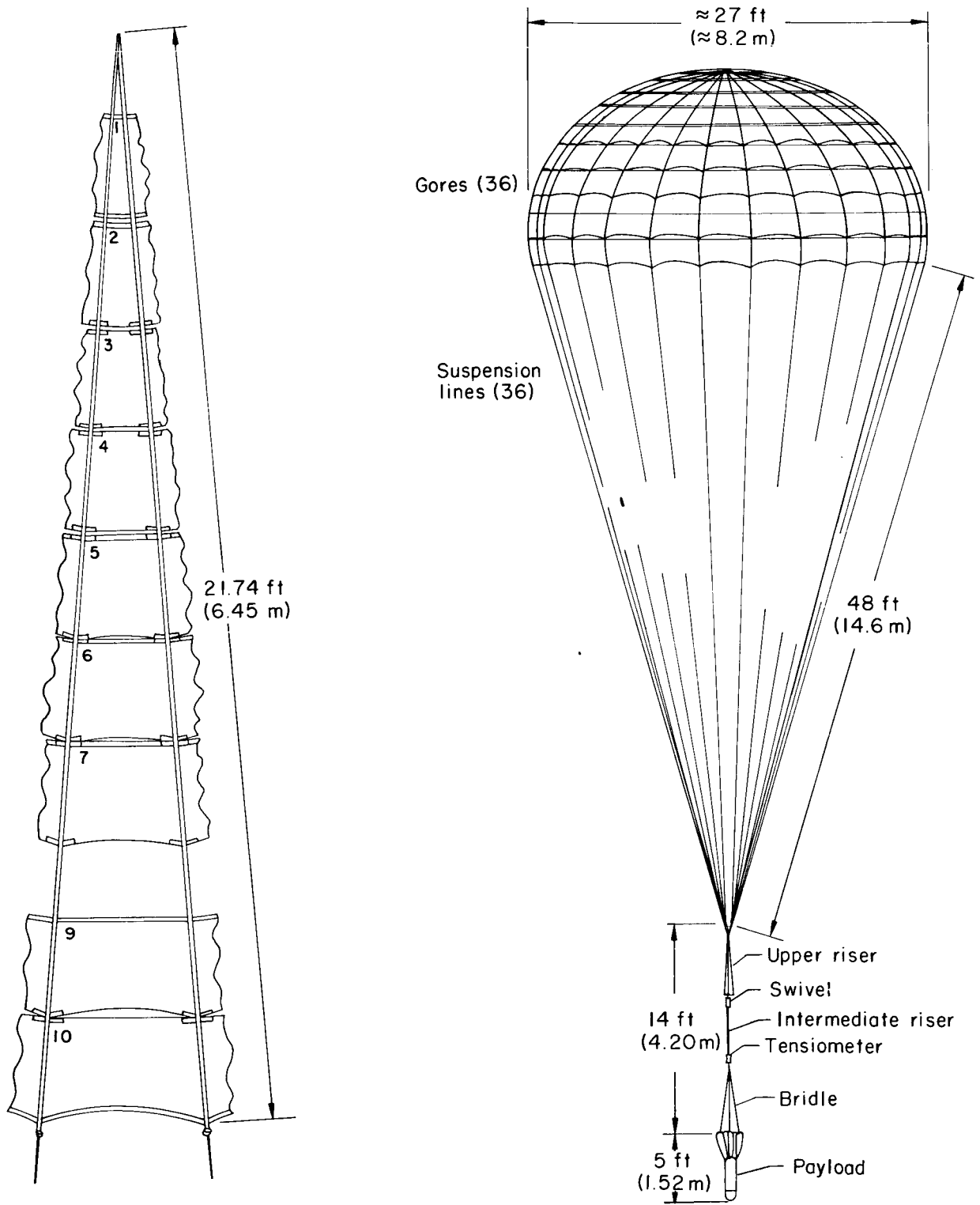


Figure 3.- Parachute-gore and flight configuration.



Figure 4.- Split cylindrical deployment bag containing the packed parachute.

L-69-8119

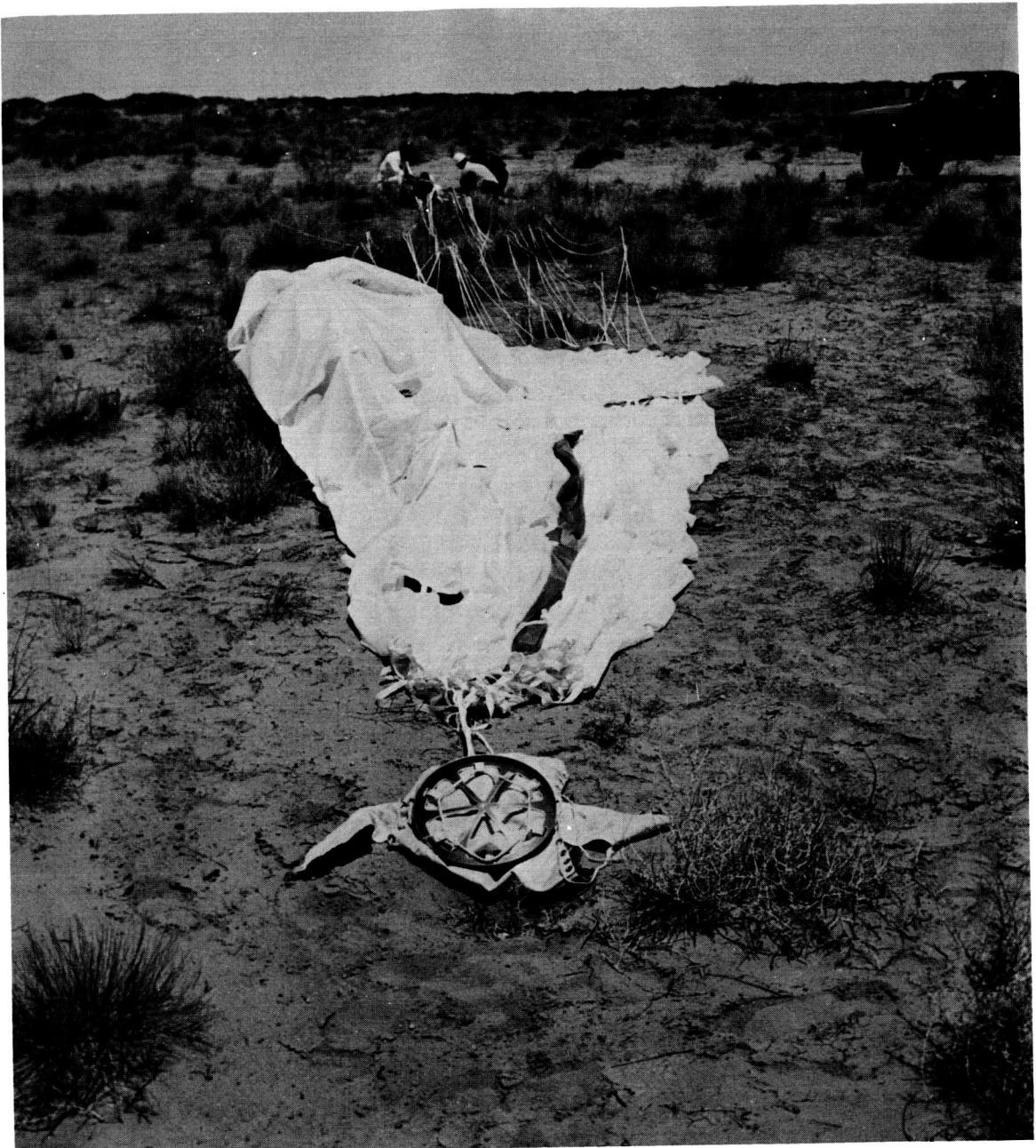
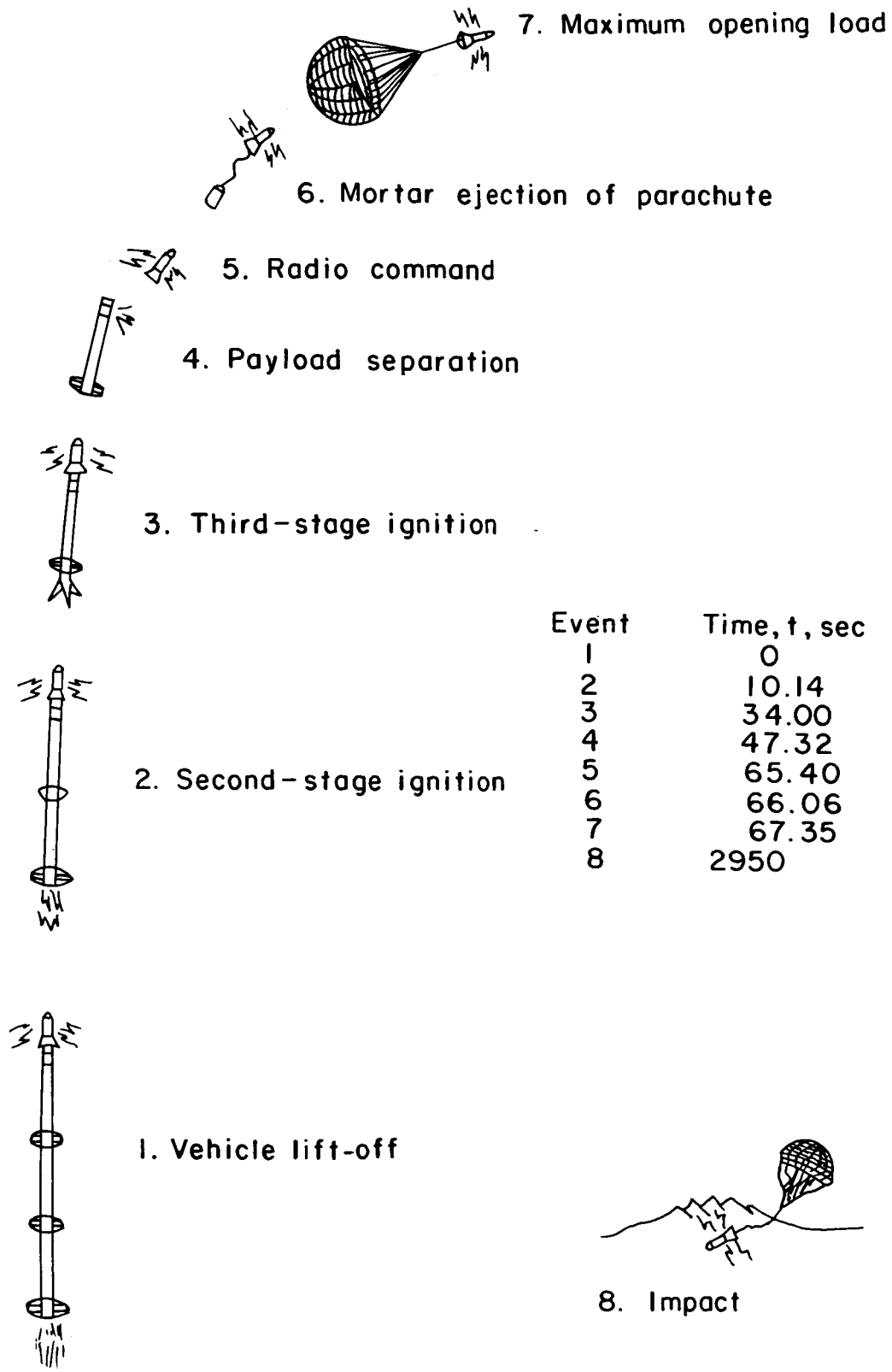


Figure 5.- Recovered parachute with attached deployment bag and mortar lid.

L-70-1590



7. Maximum opening load

6. Mortar ejection of parachute

5. Radio command

4. Payload separation

3. Third-stage ignition

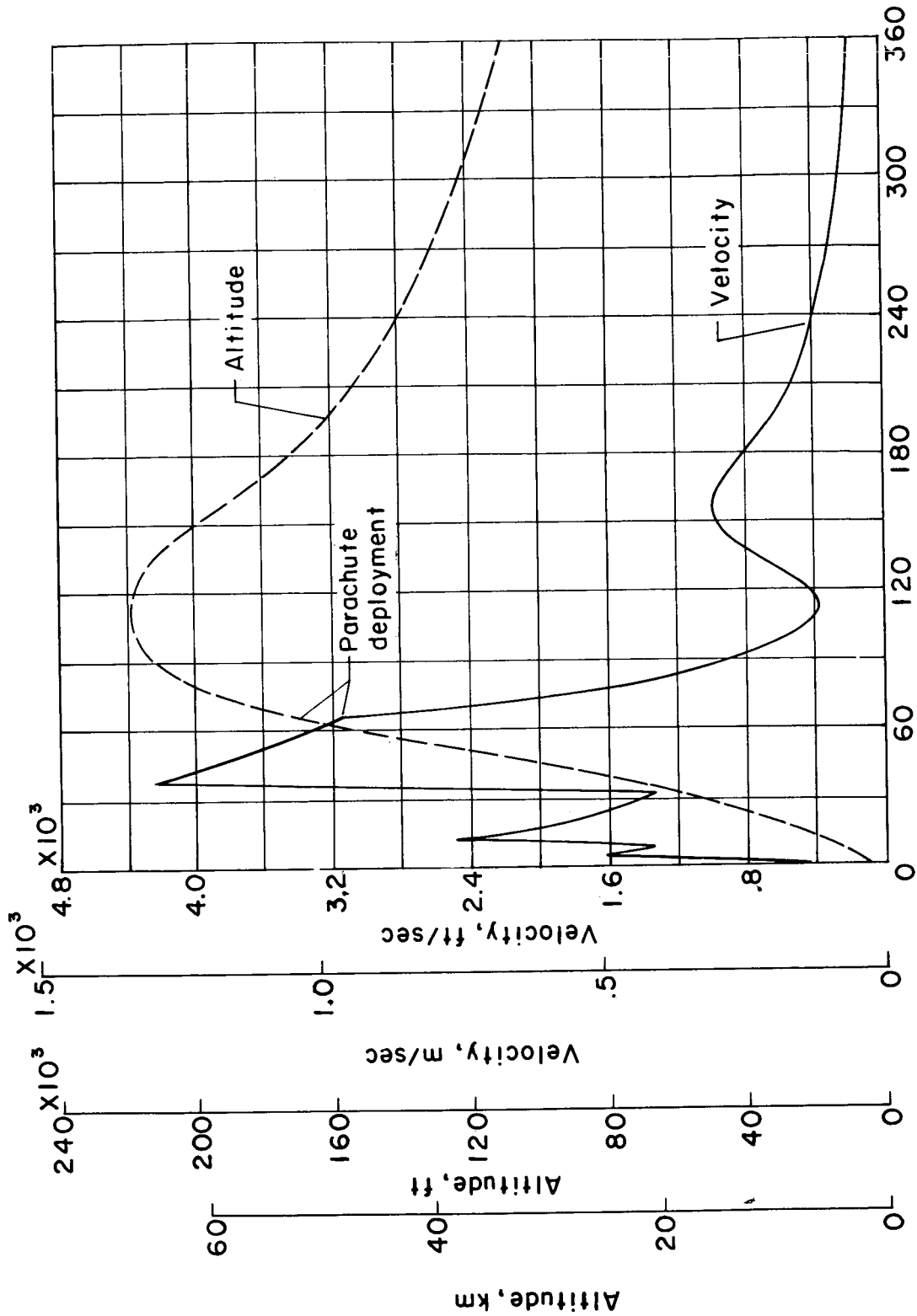
2. Second-stage ignition

1. Vehicle lift-off

Event	Time, t, sec
1	0
2	10.14
3	34.00
4	47.32
5	65.40
6	66.06
7	67.35
8	2950

8. Impact

Figure 6.- Flight sequence of events.



Time from lift-off, sec

Figure 7.- Time histories of altitude and relative velocity.

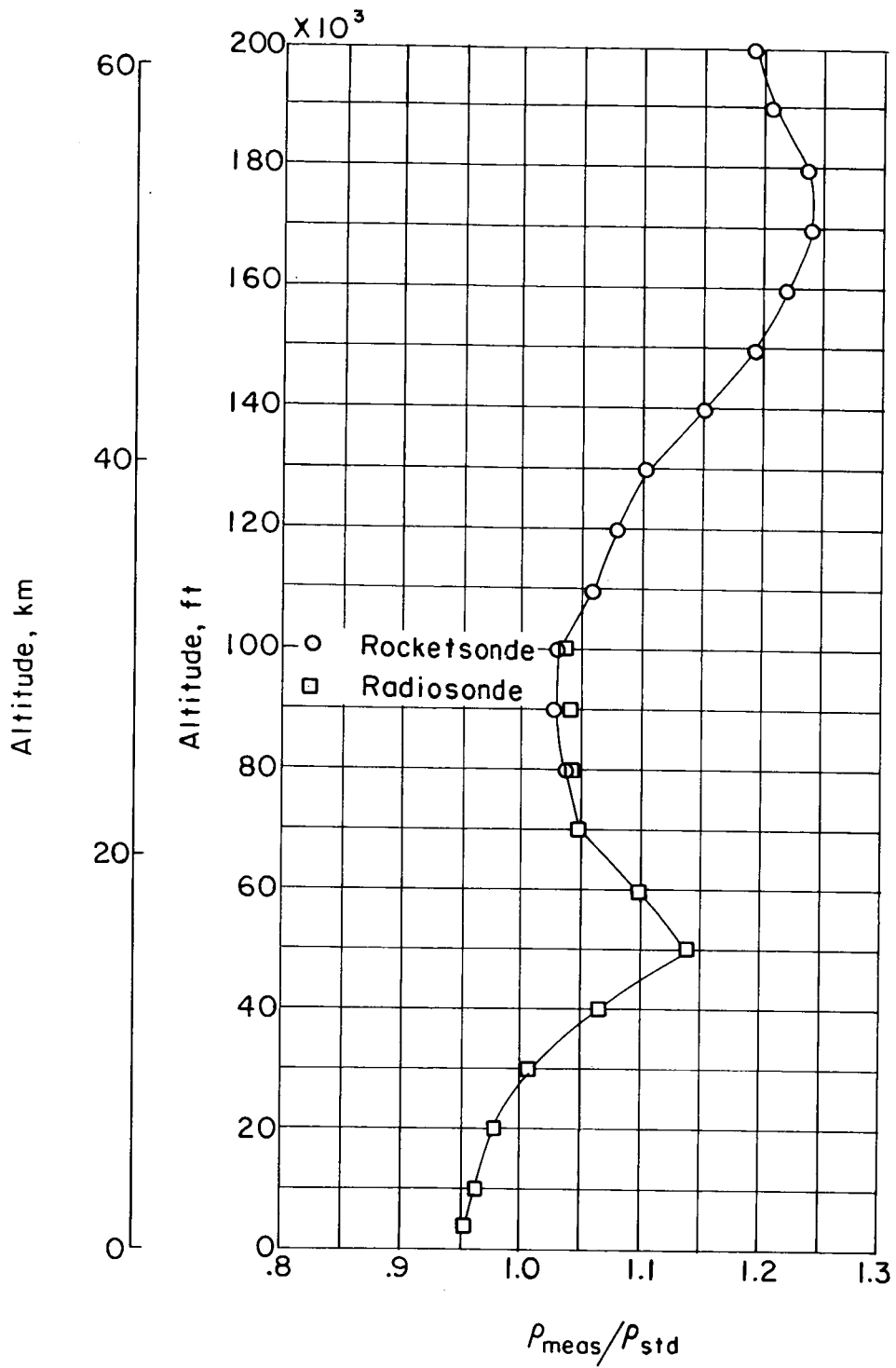


Figure 8.- Atmospheric density profile. p_{std} is the 1962 standard atmospheric density.

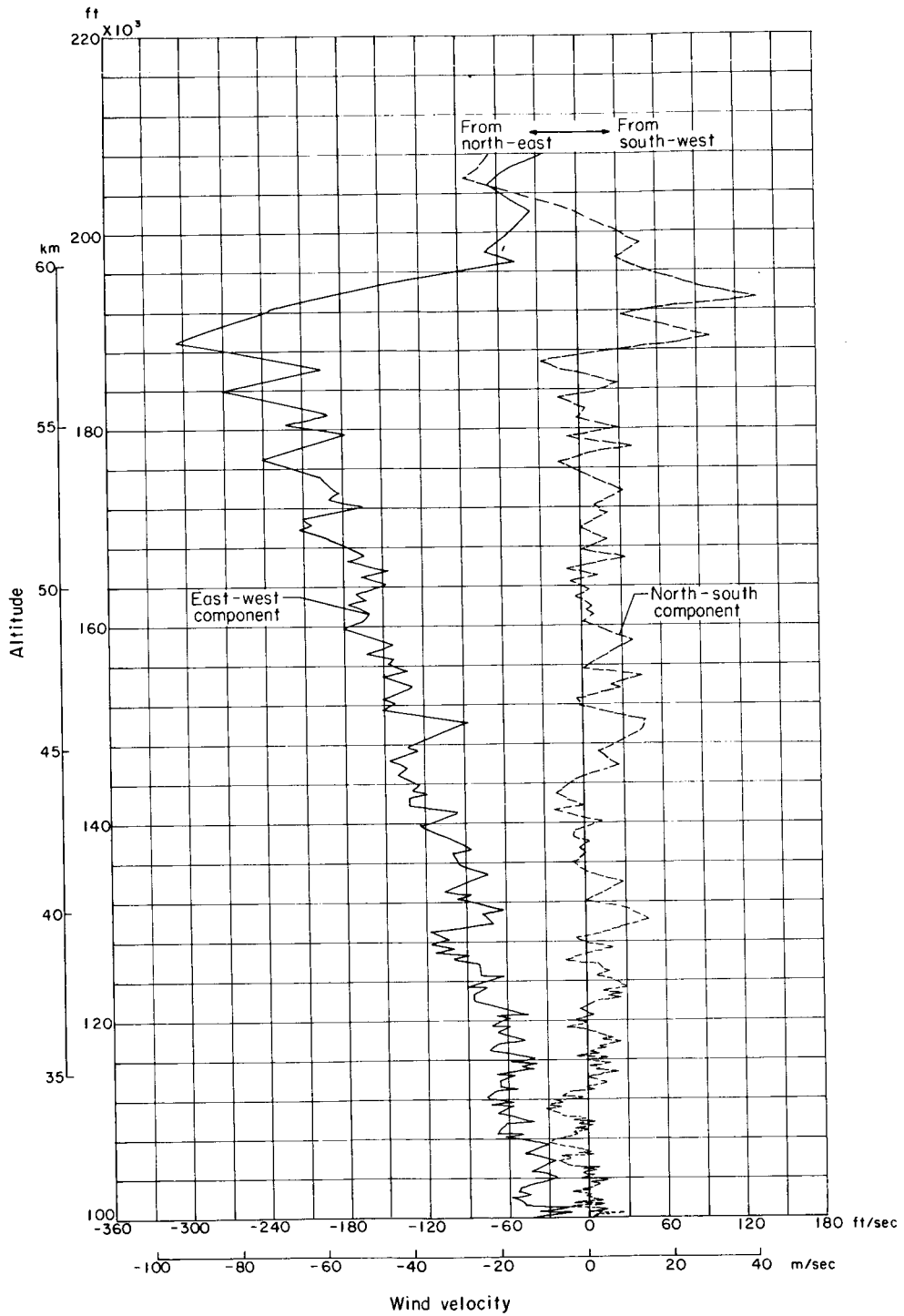


Figure 9.- Wind velocity profile in north-south and east-west components.

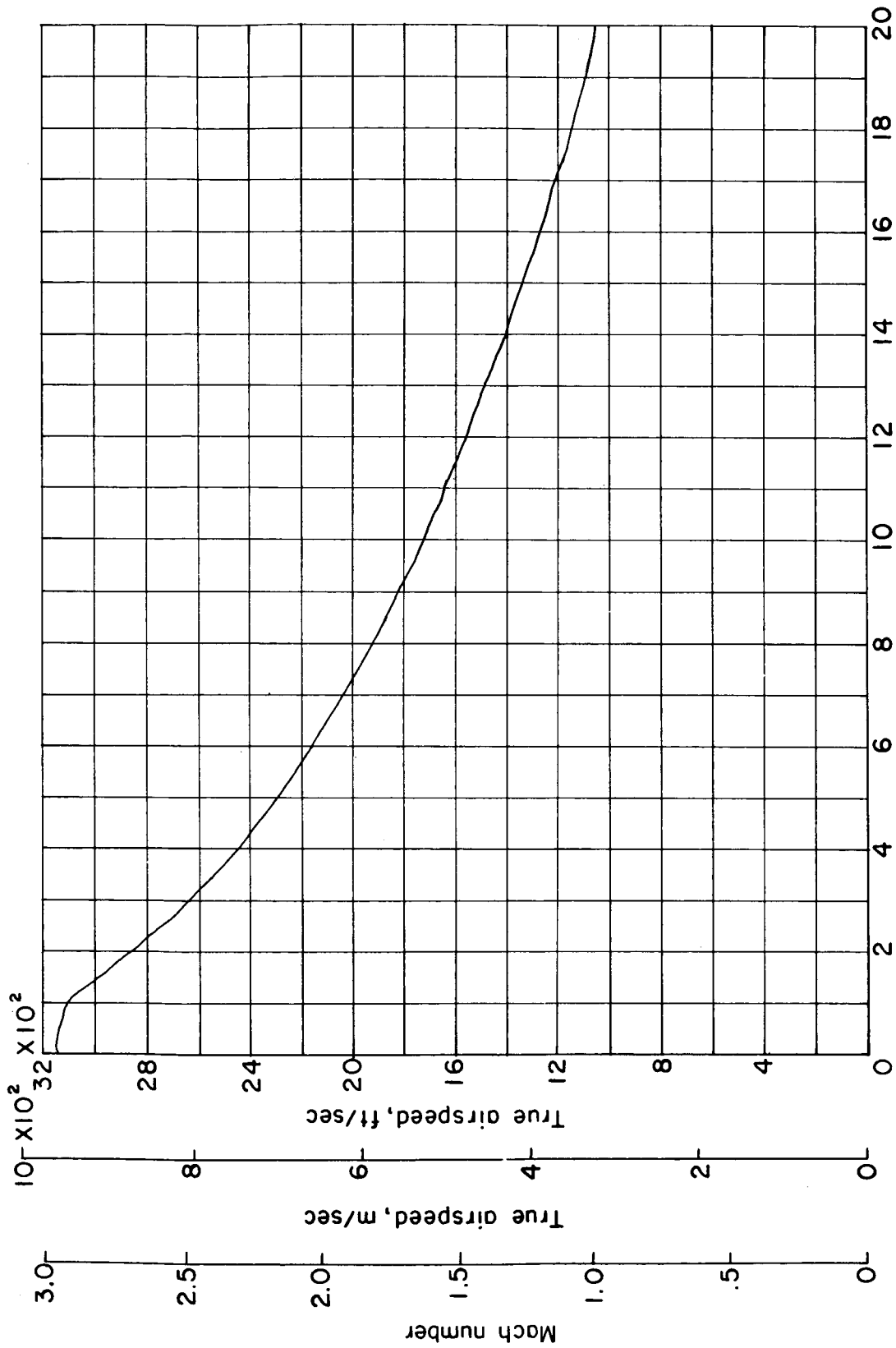


Figure 10.- Mach number and true airspeed time histories after mortar firing.

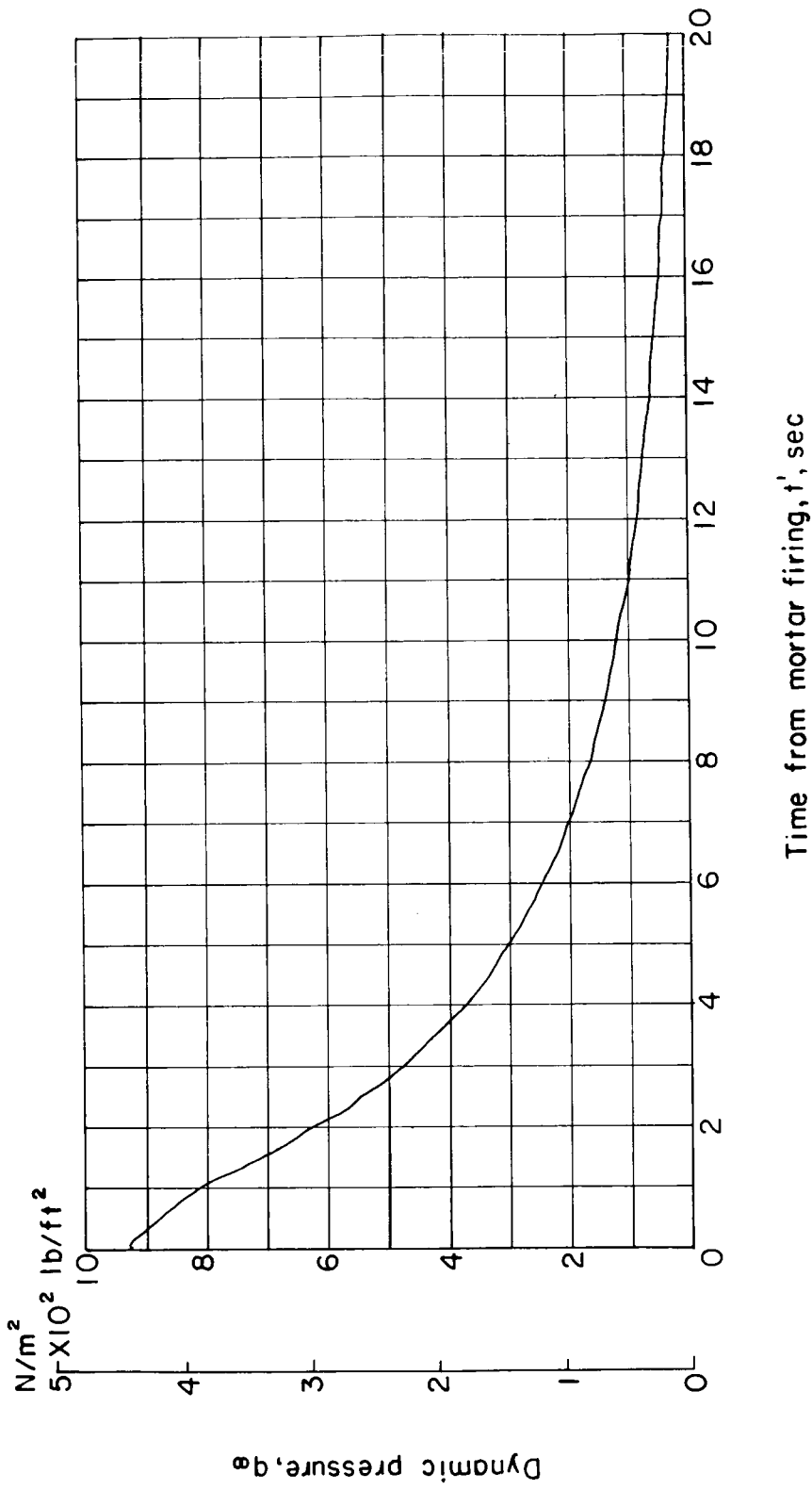


Figure 11.- Dynamic pressure time history after mortar firing.

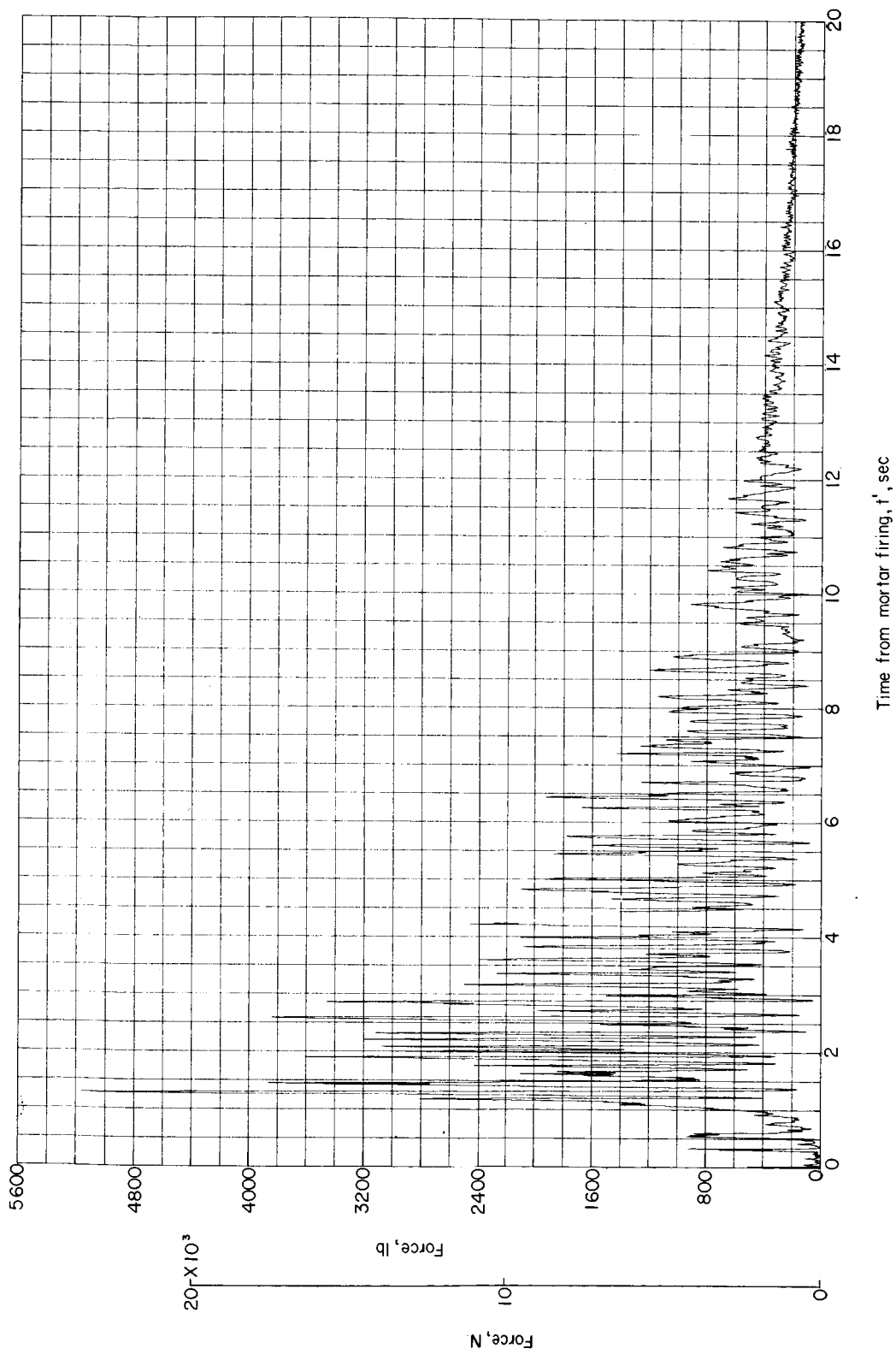


Figure 12:- Time history of force measured by the tensiometer.

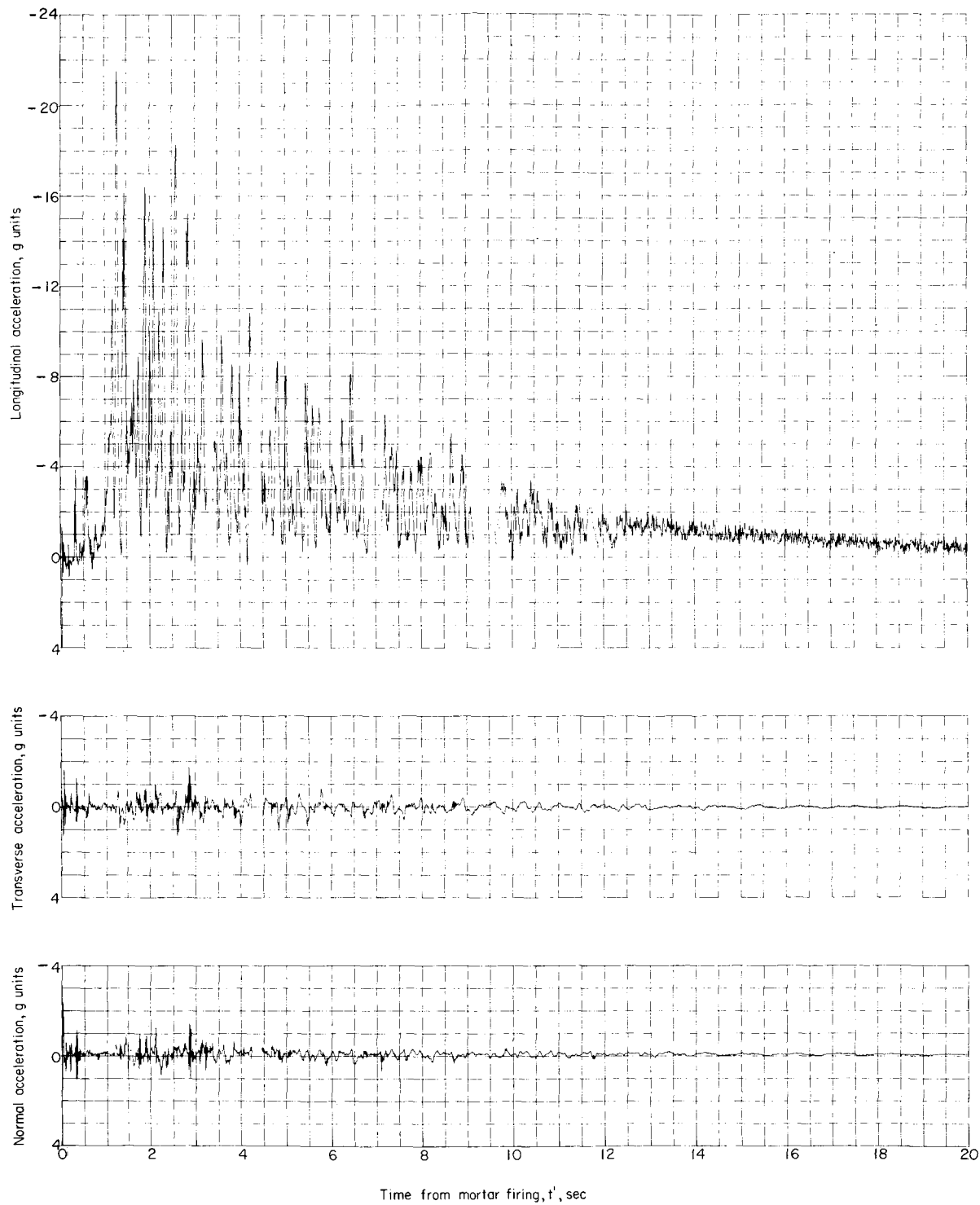


Figure 13.- Acceleration time histories.

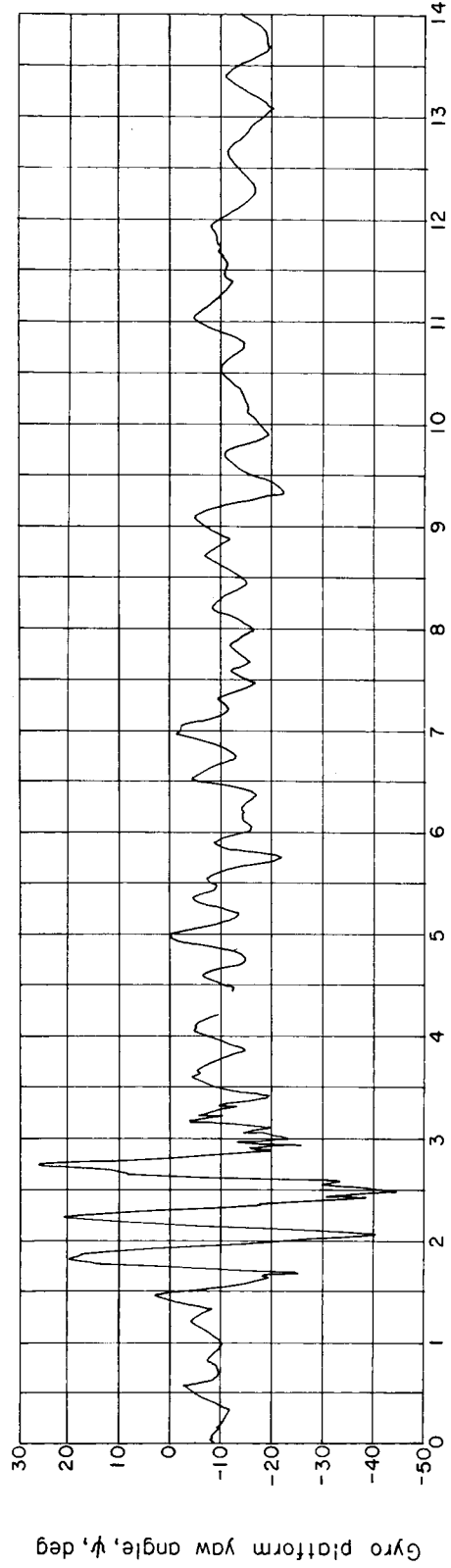
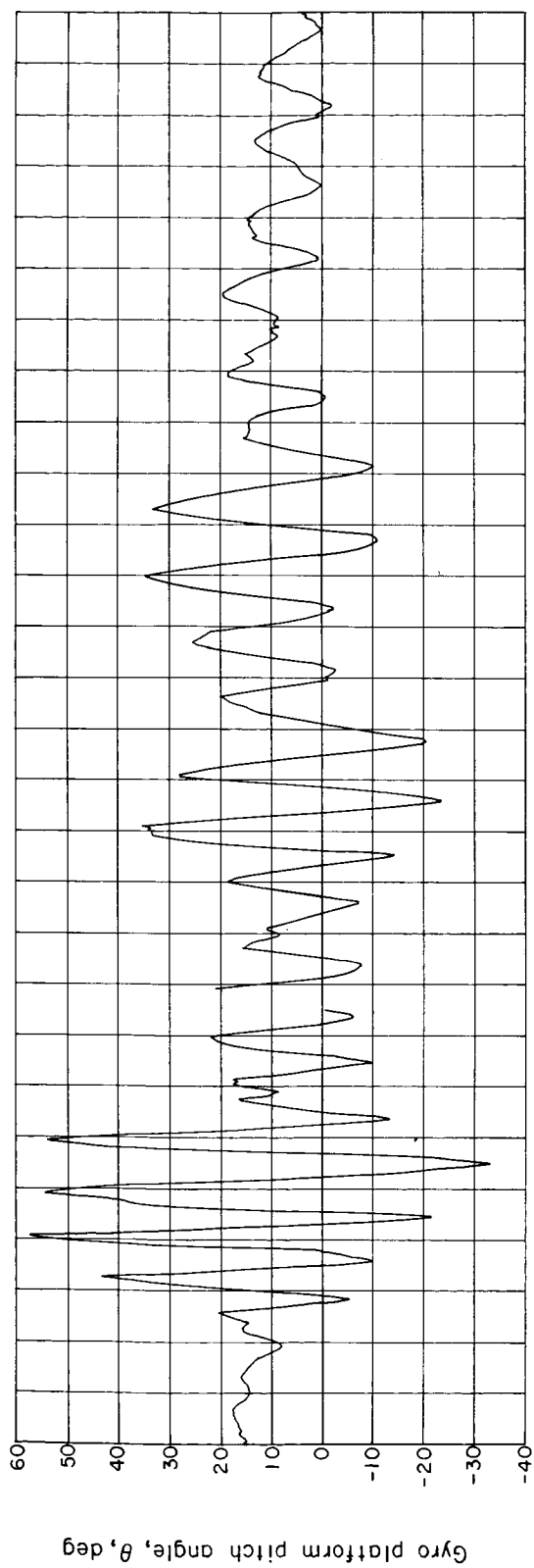


Figure 14.- Payload pitch- and yaw-angle time histories.

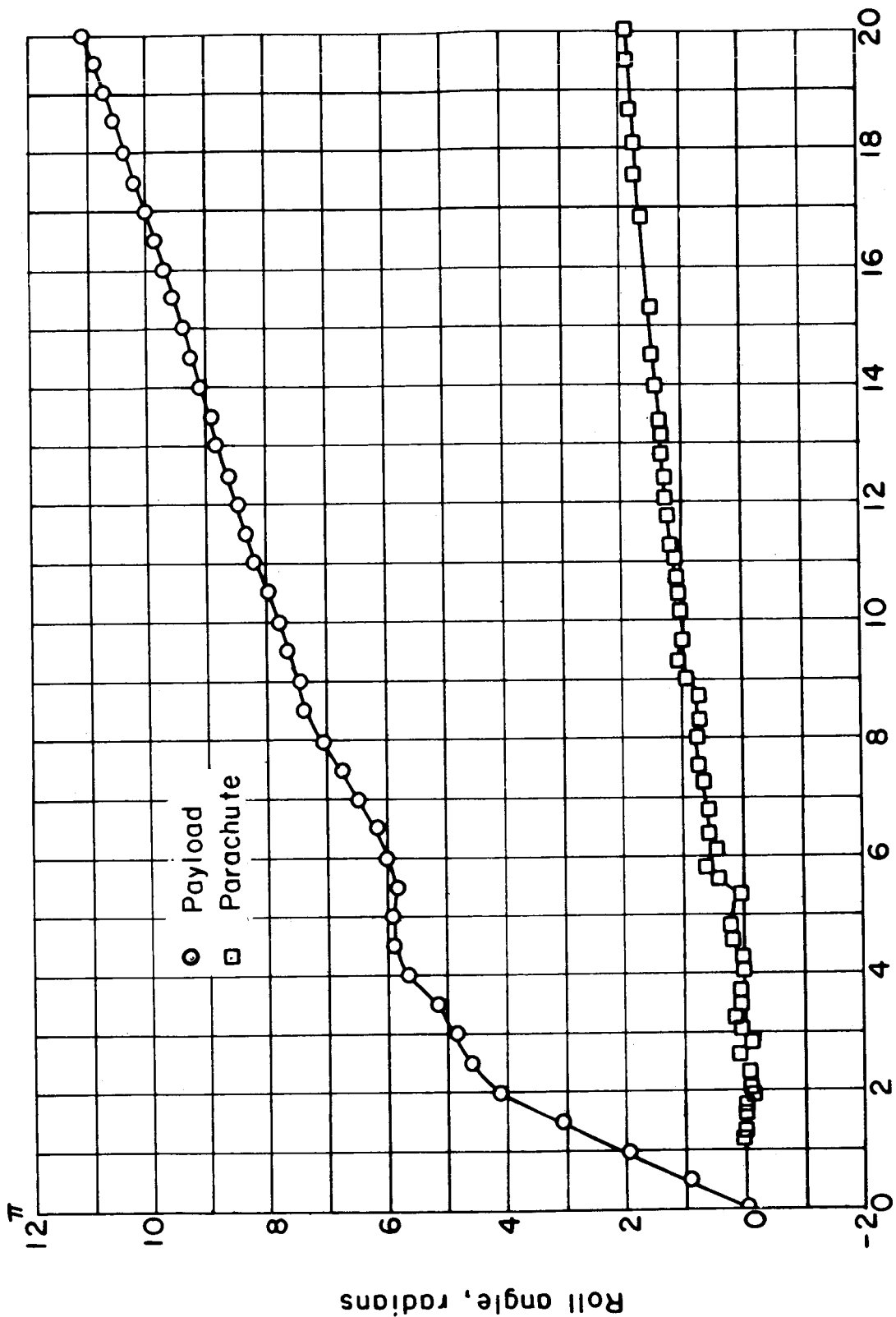
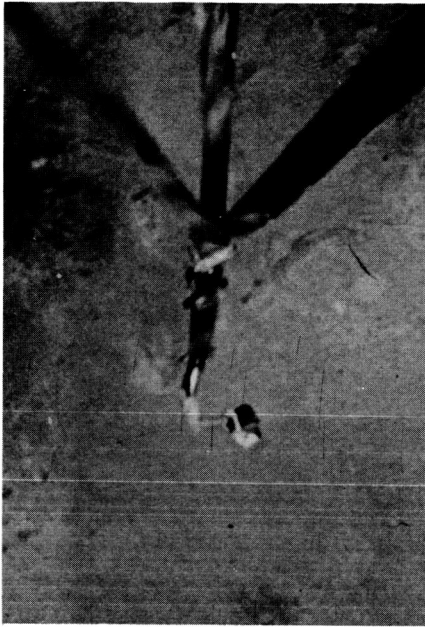


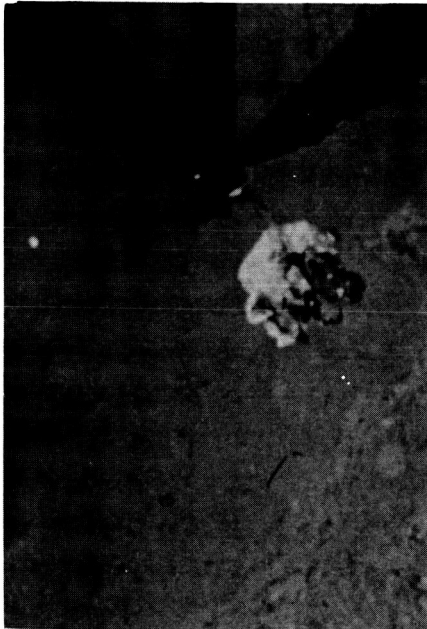
Figure 15.- Payload and parachute roll-angle histories.



$t' = 0.54 \text{ sec}$



$t' = 0.70 \text{ sec}$



$t' = 0.86 \text{ sec}$

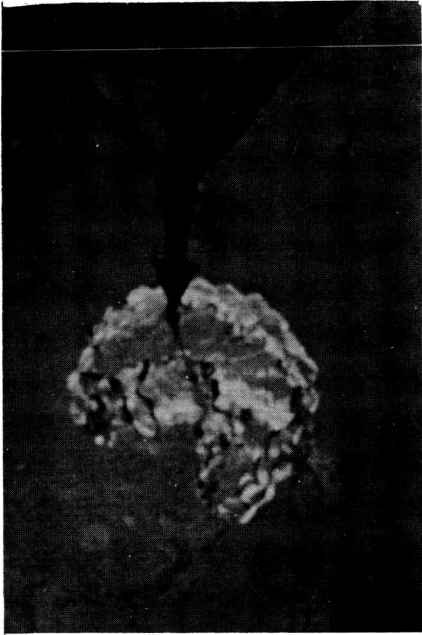


$t' = 0.97 \text{ sec}$

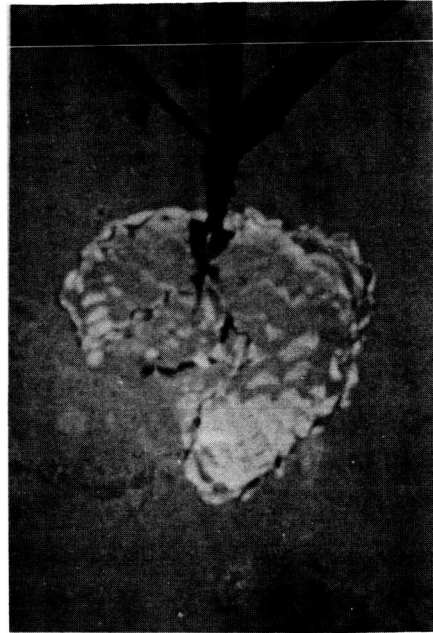
(a) Initial canopy inflation sequence.

L-70-1591

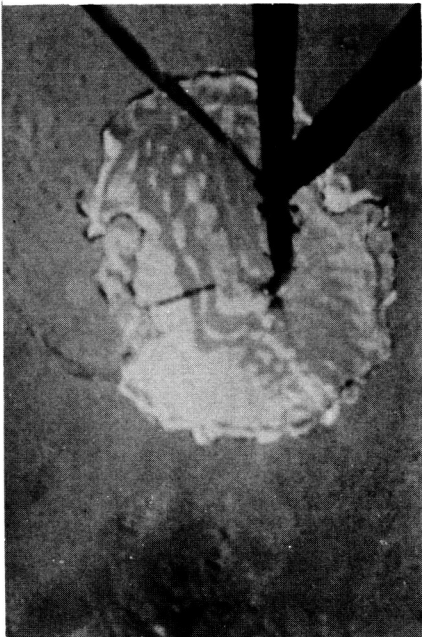
Figure 16.- Onboard camera photographs.



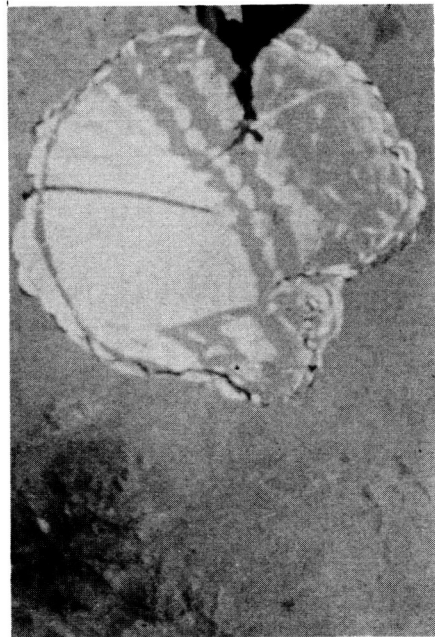
$t' = 1.05 \text{ sec}$



$t' = 1.11 \text{ sec}$



$t' = 1.19 \text{ sec}$

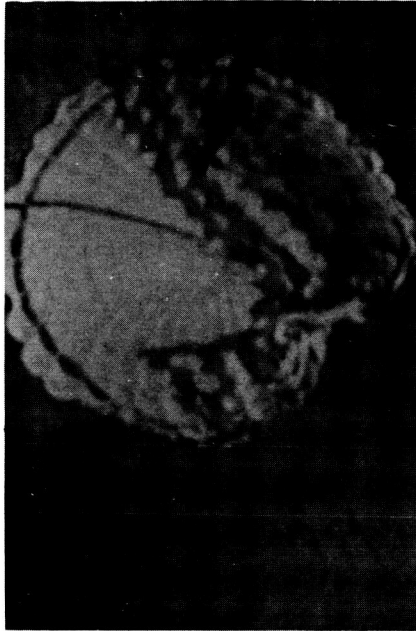


$t' = 1.25 \text{ sec}$

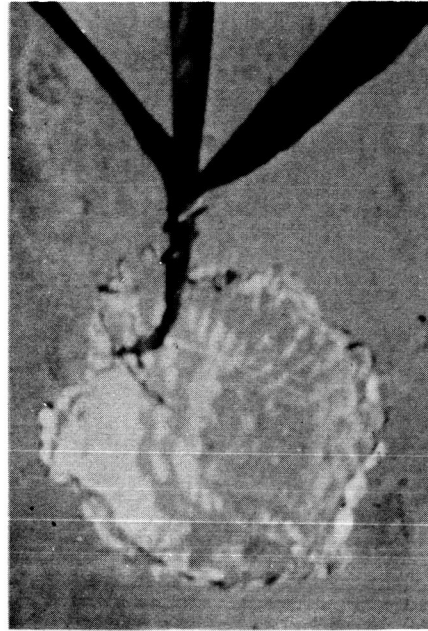
(a) Concluded.

L-70-1592

Figure 16.- Continued.



$t' = 1.27 \text{ sec}$



$t' = 1.33 \text{ sec}$



$t' = 1.41 \text{ sec}$

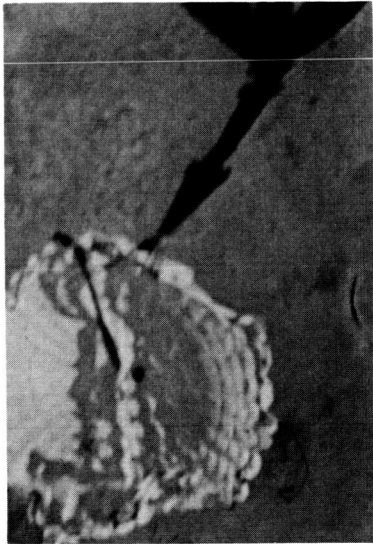


$t' = 1.69 \text{ sec}$

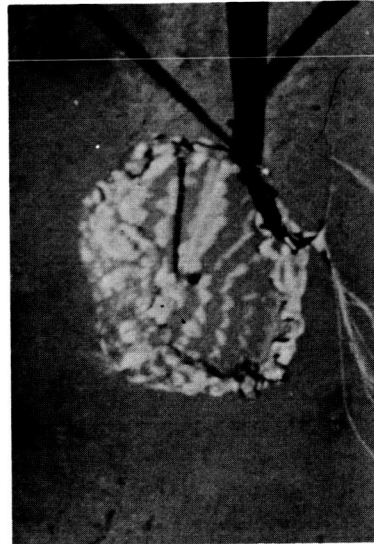
(b) Canopy collapse sequence.

L-70-1593

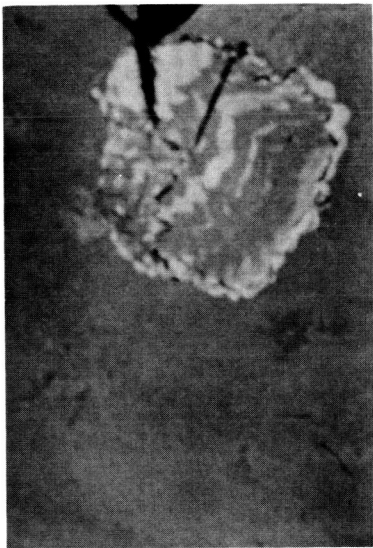
Figure 16.- Continued.



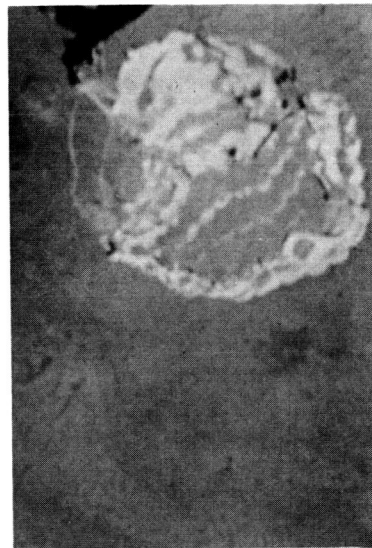
$t' = 3.17$ sec
Tensiometer force
2499 lb (11116 N)



$t' = 3.28$ sec
Tensiometer force
454 lb (2019 N)



$t' = 3.36$ sec
Tensiometer force
2277 lb (10128 N)



$t' = 3.41$ sec
Tensiometer force
581 lb (2584 N)

(c) Canopy load variation sequence.

L-70-1594

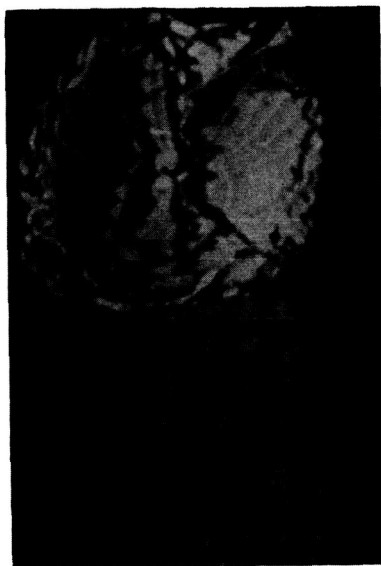
Figure 16.- Continued.



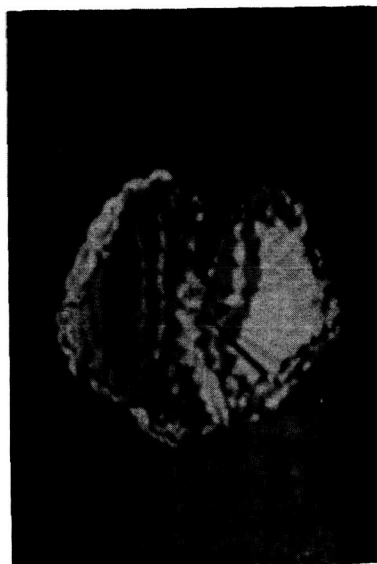
$t' = 4.73 \text{ sec}$
Tensiometer force
292 lb (1299 N)



$t' = 4.83 \text{ sec}$
Tensiometer force
2093 lb (9310 N)



$t' = 4.94 \text{ sec}$
Tensiometer force
170 lb (756 N)

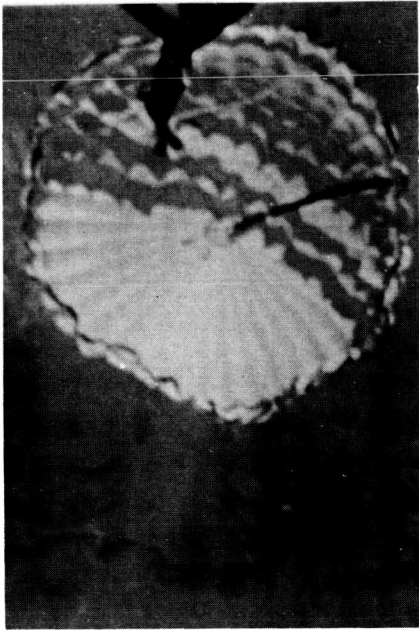


$t' = 5.02 \text{ sec}$
Tensiometer force
1900 lb (8451 N)

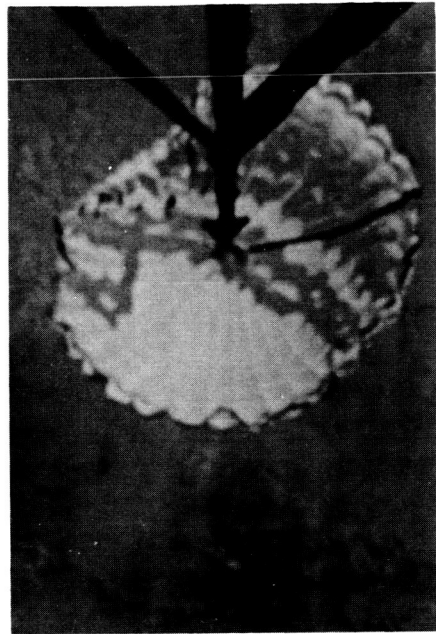
(c) Concluded.

L-70-1595

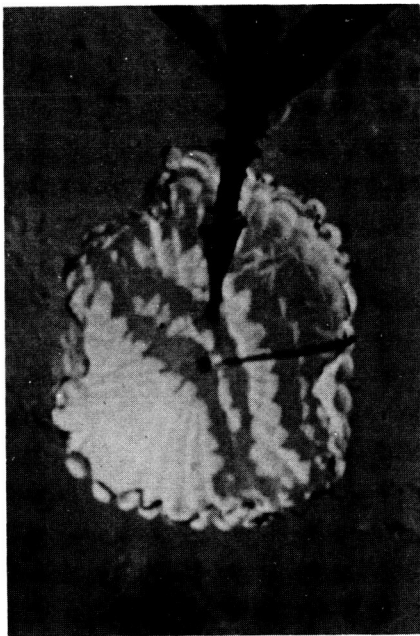
Figure 16.- Continued.



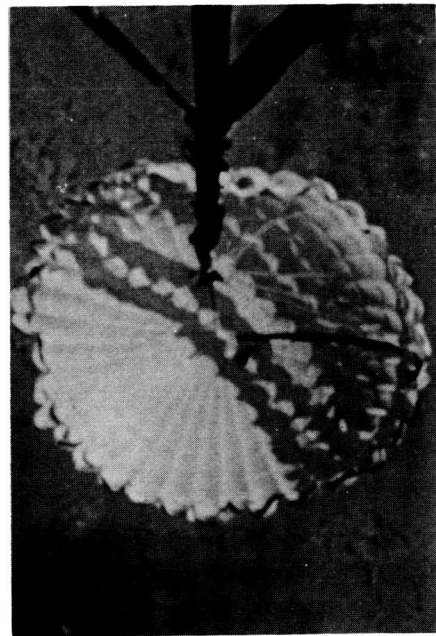
$t' = 11.75 \text{ sec}$



$t' = 12.00 \text{ sec}$



$t' = 12.25 \text{ sec}$

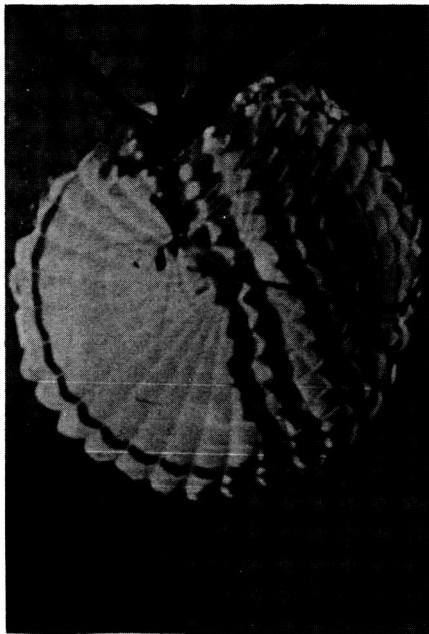


$t' = 12.50 \text{ sec}$

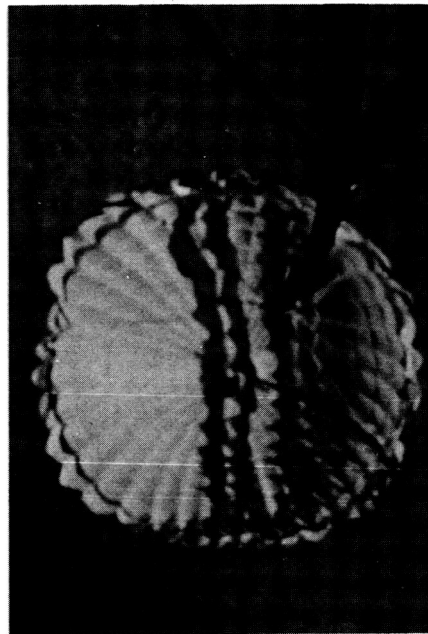
(d) Canopy inflation stabilization sequence.

L-70-1596

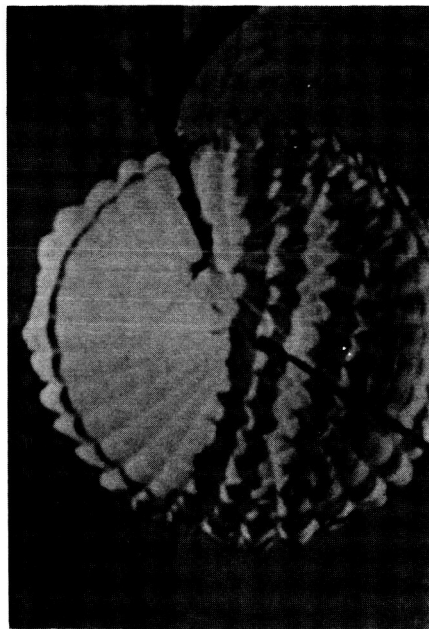
Figure 16.- Continued.



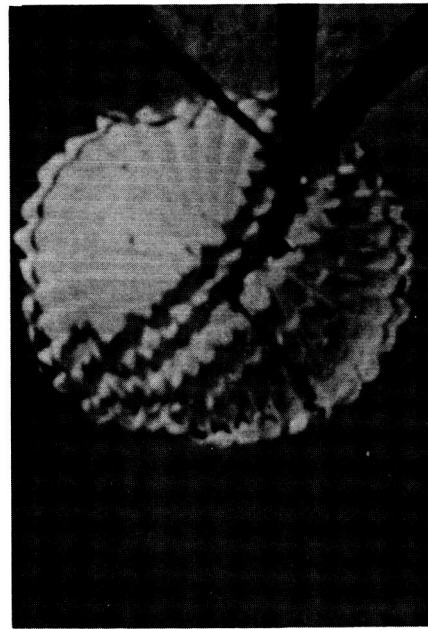
$t' = 12.75 \text{ sec}$



$t' = 13.00 \text{ sec}$



$t' = 13.38 \text{ sec}$

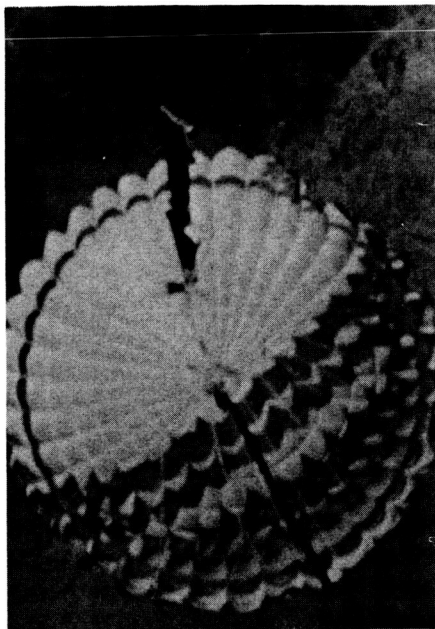


$t' = 13.75 \text{ sec}$

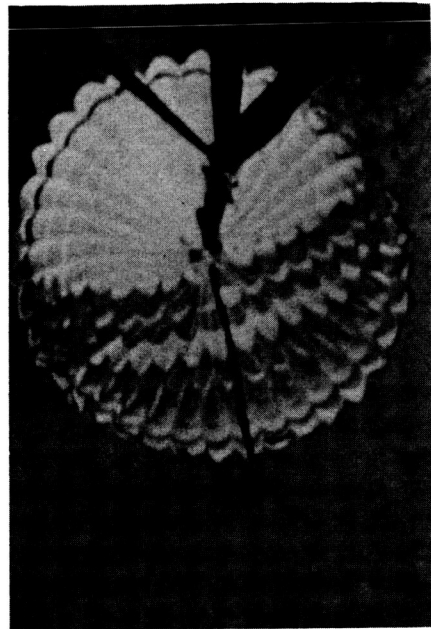
(d) Continued.

L-70-1597

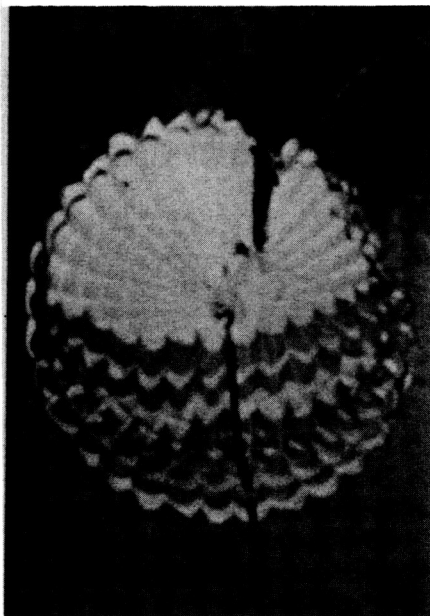
Figure 16.- Continued.



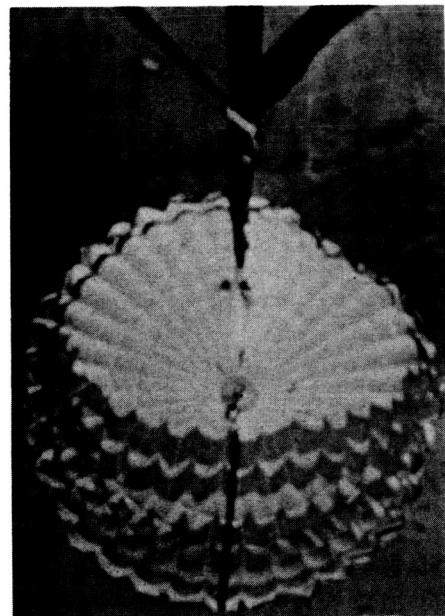
$t' = 14.16 \text{ sec}$



$t' = 14.50 \text{ sec}$



$t' = 14.75 \text{ sec}$

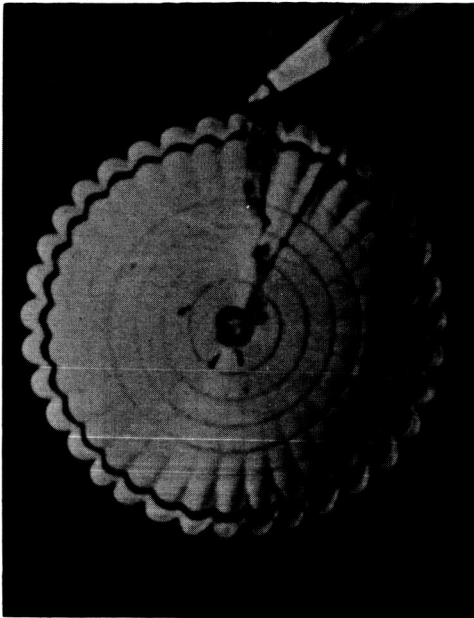


$t' = 15.00 \text{ sec}$

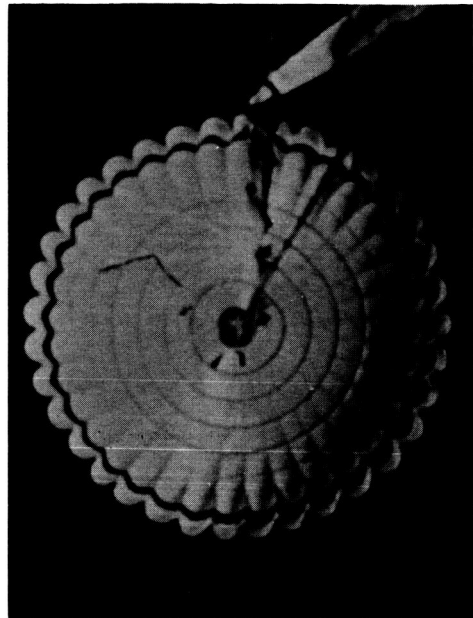
(d) Concluded.

L-70-1598

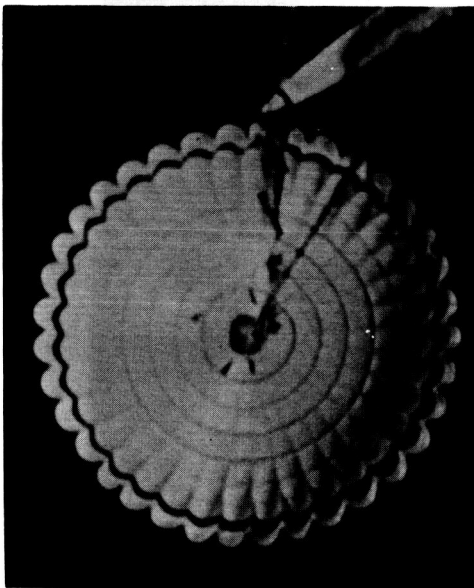
Figure 16.- Continued.



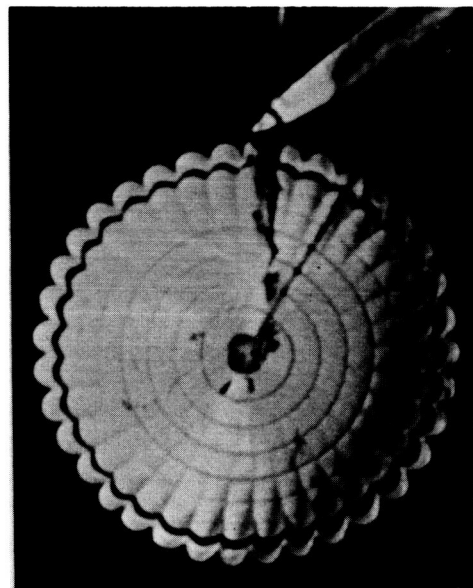
$t' = 51.75 \text{ sec}$



$t' = 51.77 \text{ sec}$



$t' = 51.78 \text{ sec}$



$t' = 51.80 \text{ sec}$

(e) Steady-state inflation.

L-70-1600

Figure 16.- Concluded.

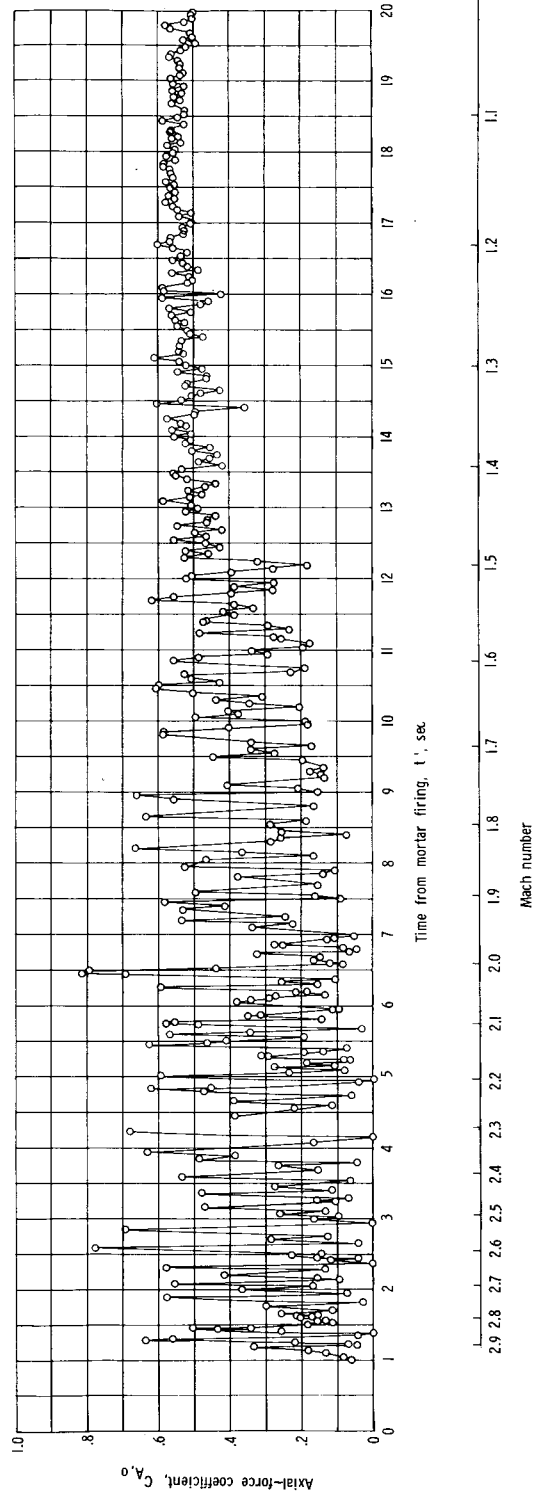
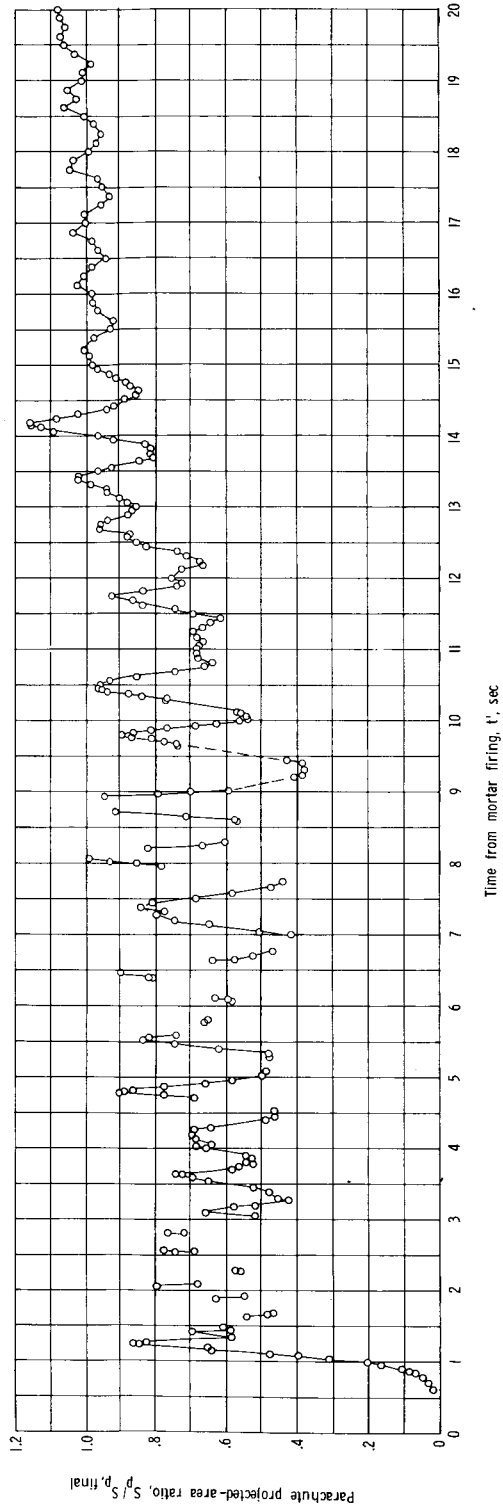


Figure 17.- Parachute projected-area ratio and axial-force coefficient as a function of time and Mach number.

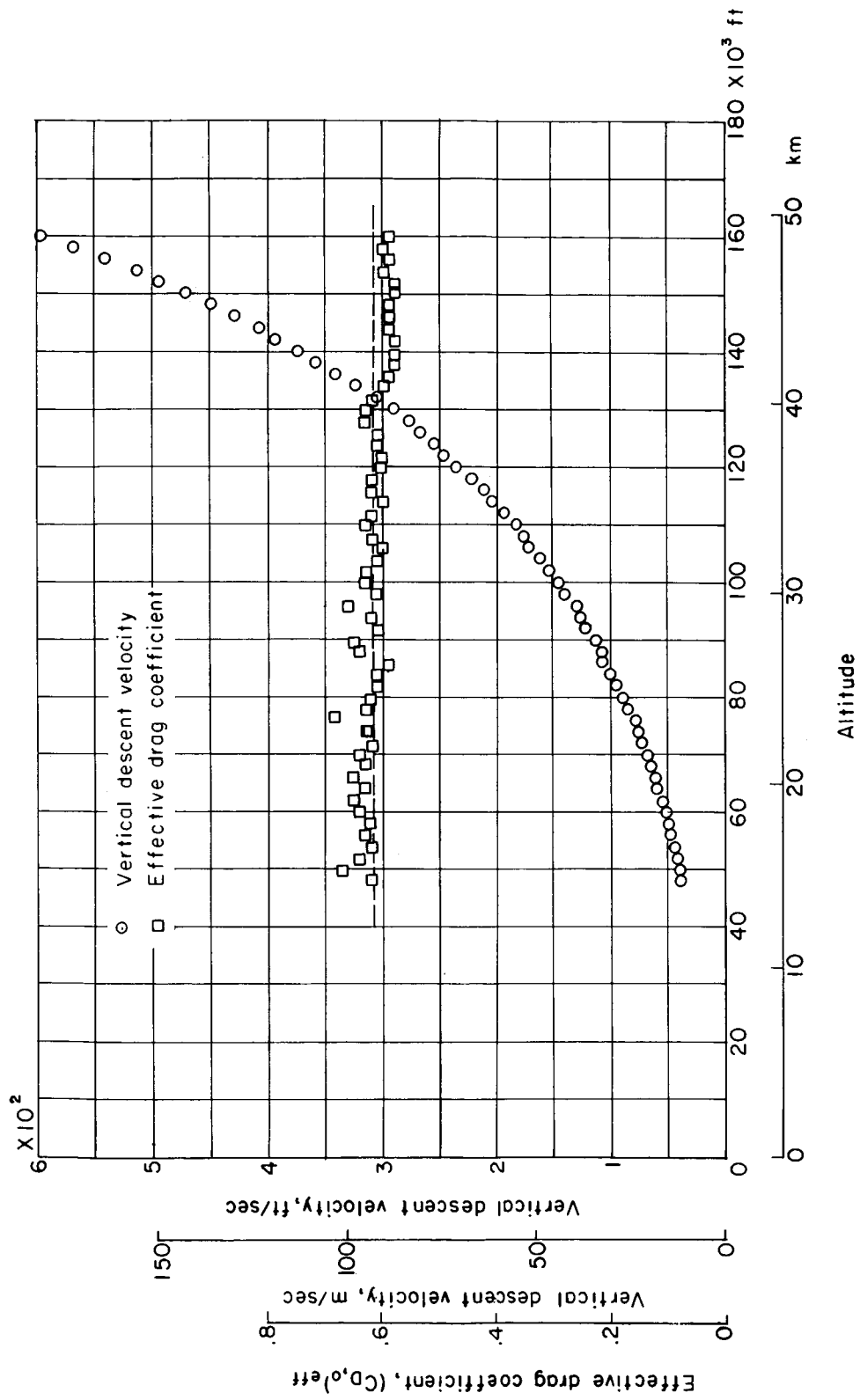


Figure 18.- Variation of vertical descent velocity and effective drag coefficient with altitude.

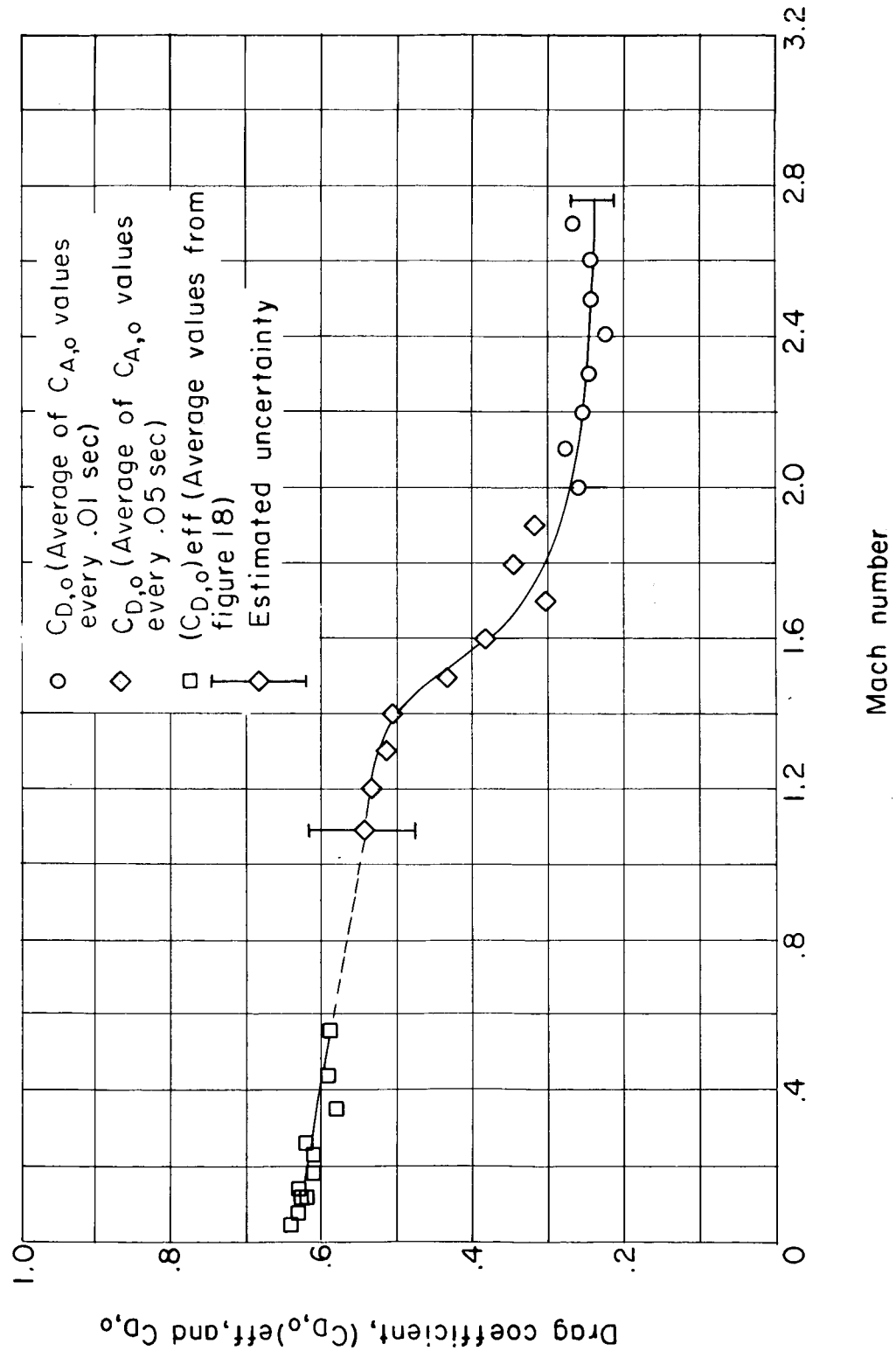


Figure 19.- Drag coefficients $(C_{D,0})_{eff}$ and $C_{D,0}$ as functions of Mach number.

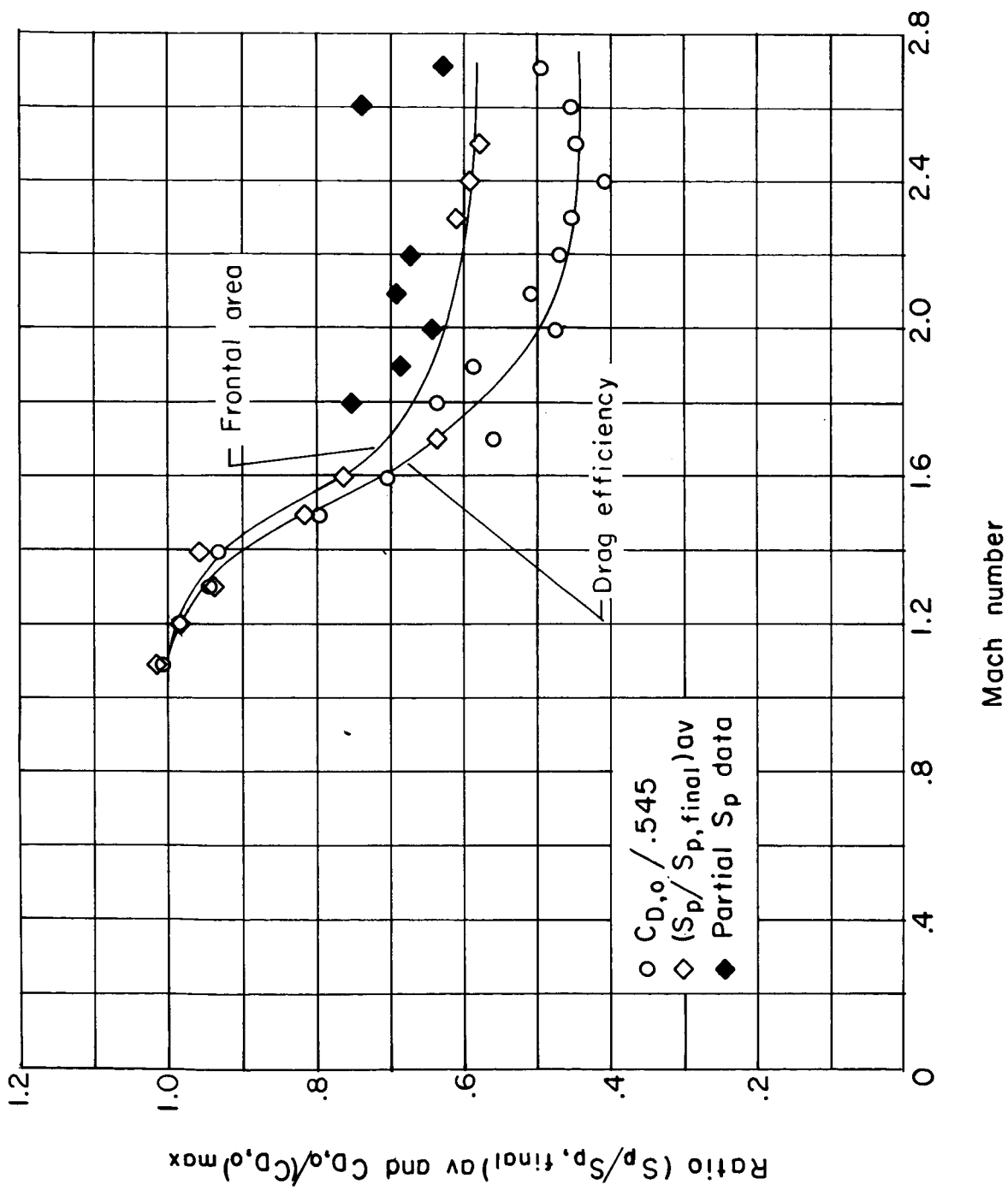


Figure 20.- Parachute frontal area and drag efficiency changes with Mach number.

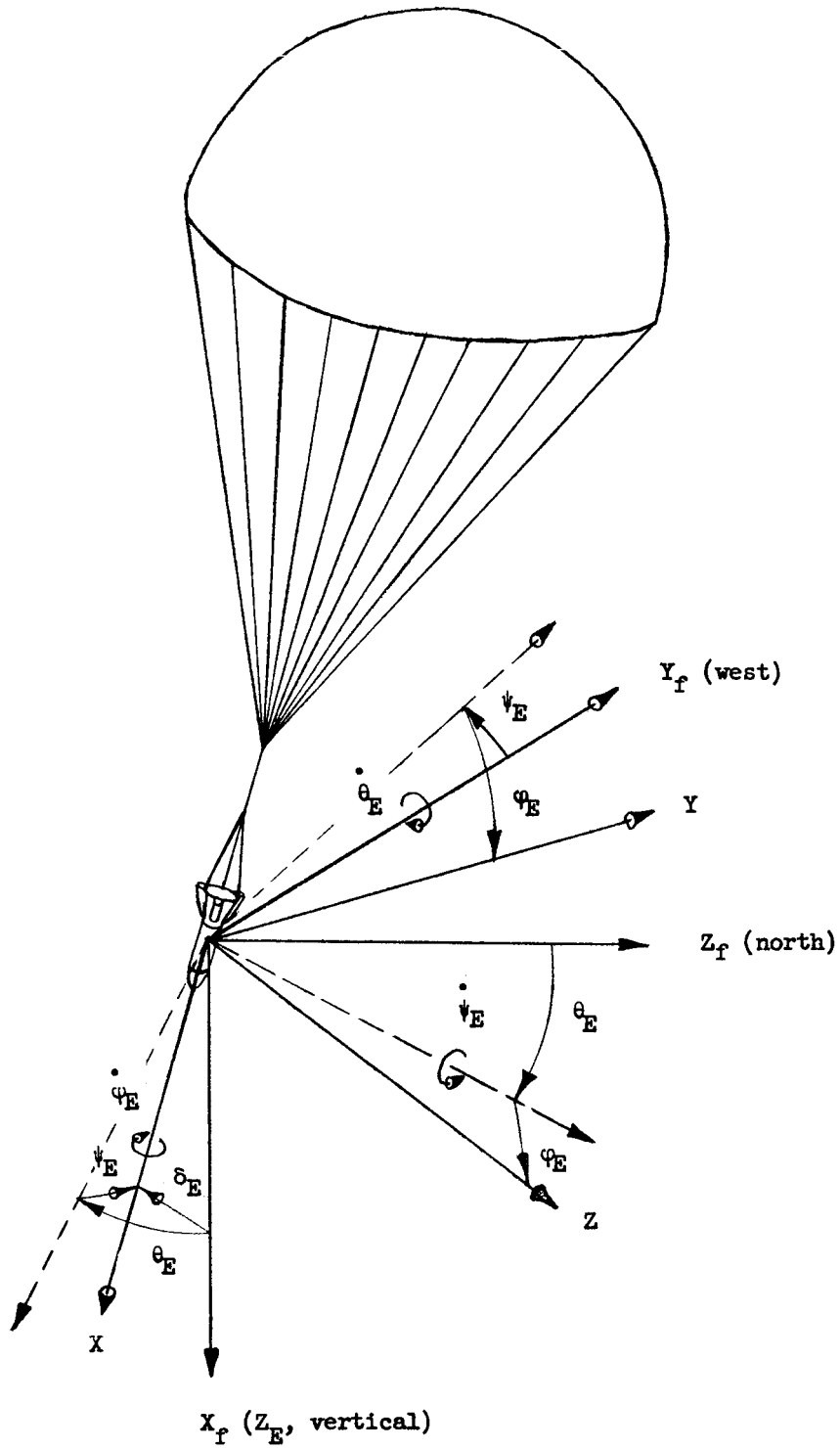


Figure 21. Sketch showing relationship between body axes (X, Y, Z) and earth-fixed axes (X_f, Y_f, Z_f) .

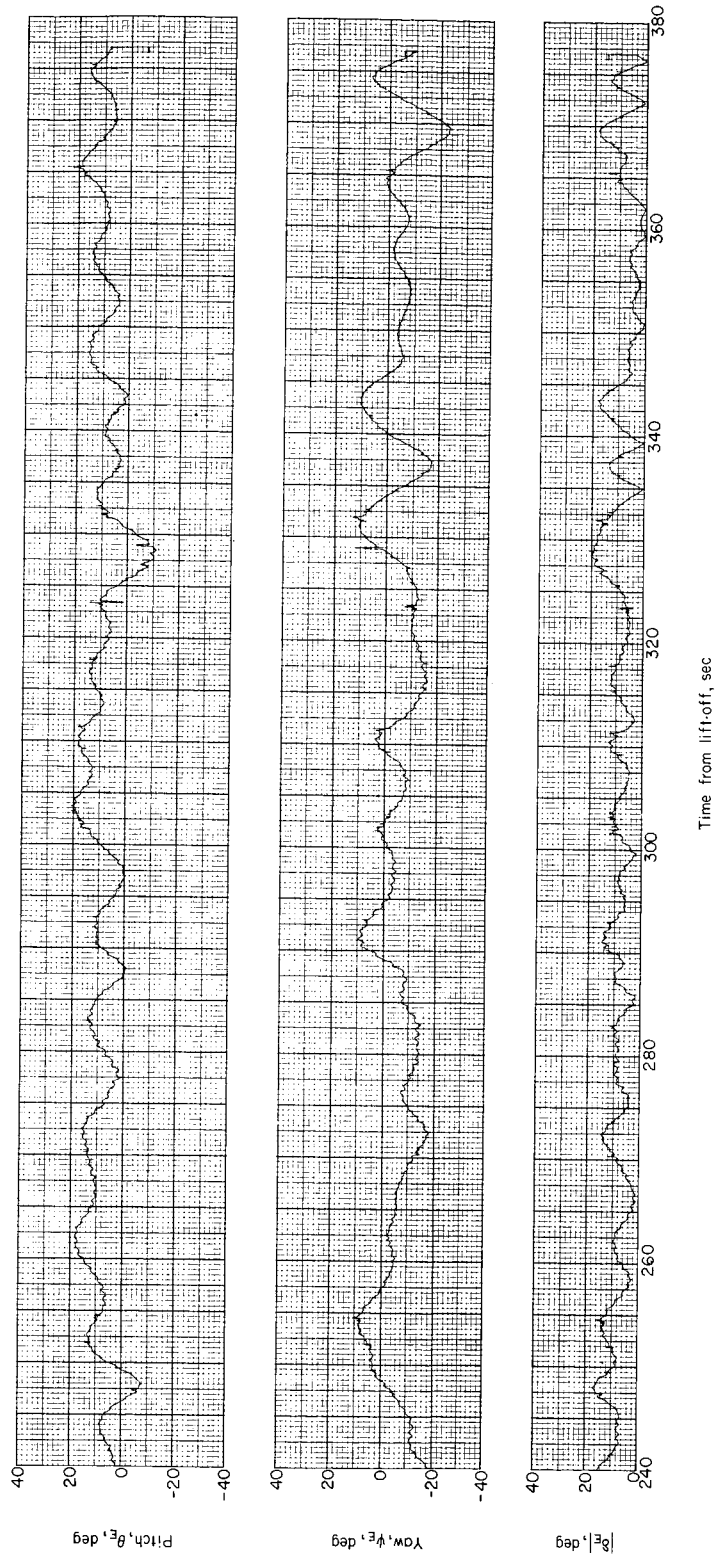


Figure 22.- Time histories of pitch θ_E , yaw ψ_E , and the magnitude of the resultant angular displacement δ_E of the payload from the local vertical for a portion of the descent trajectory from 136 500 feet (41.6 km) to 109 500 feet (33.4 km).

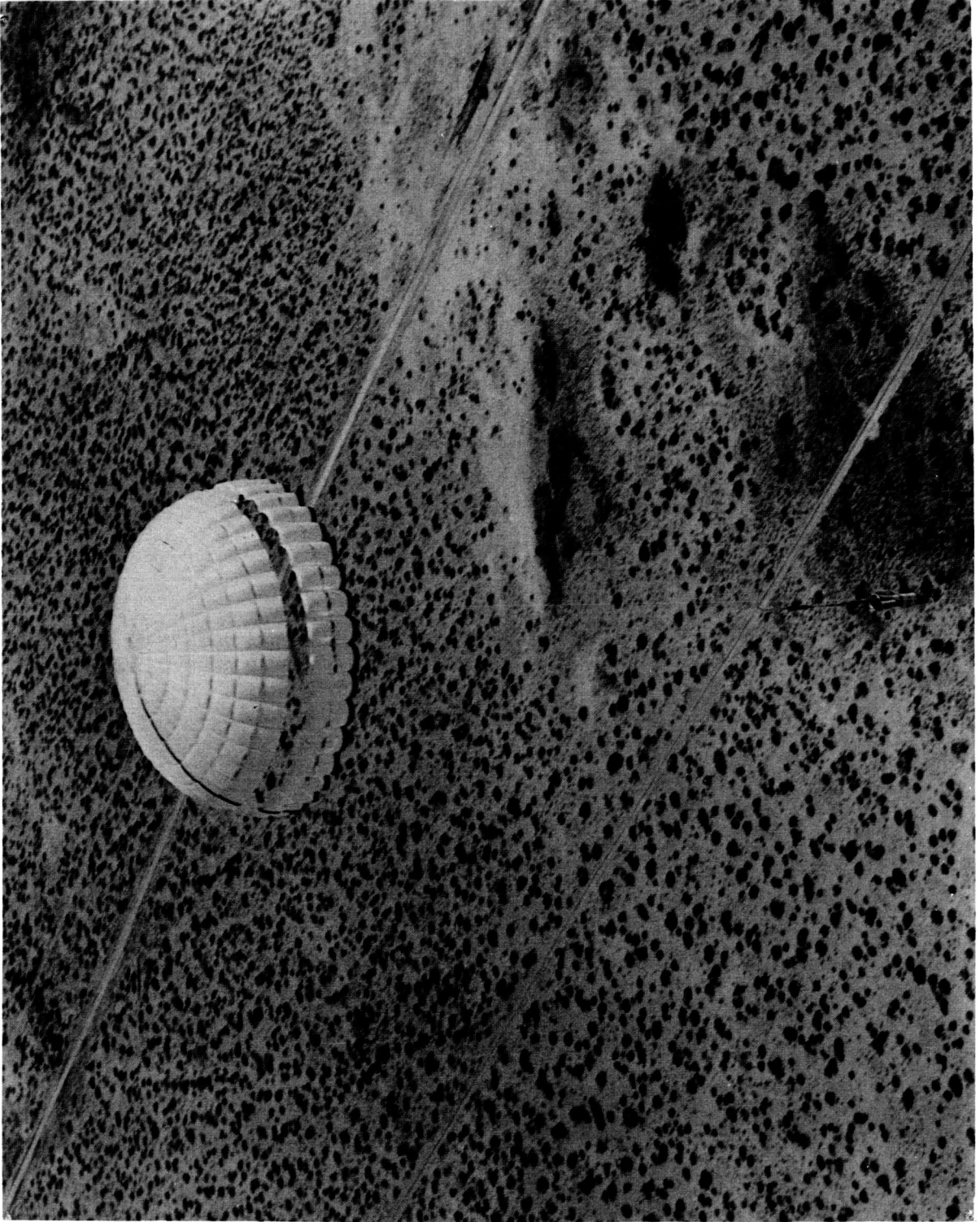


Figure 23.- Photograph of the modified ringsail parachute during descent near impact.

L-70-1599

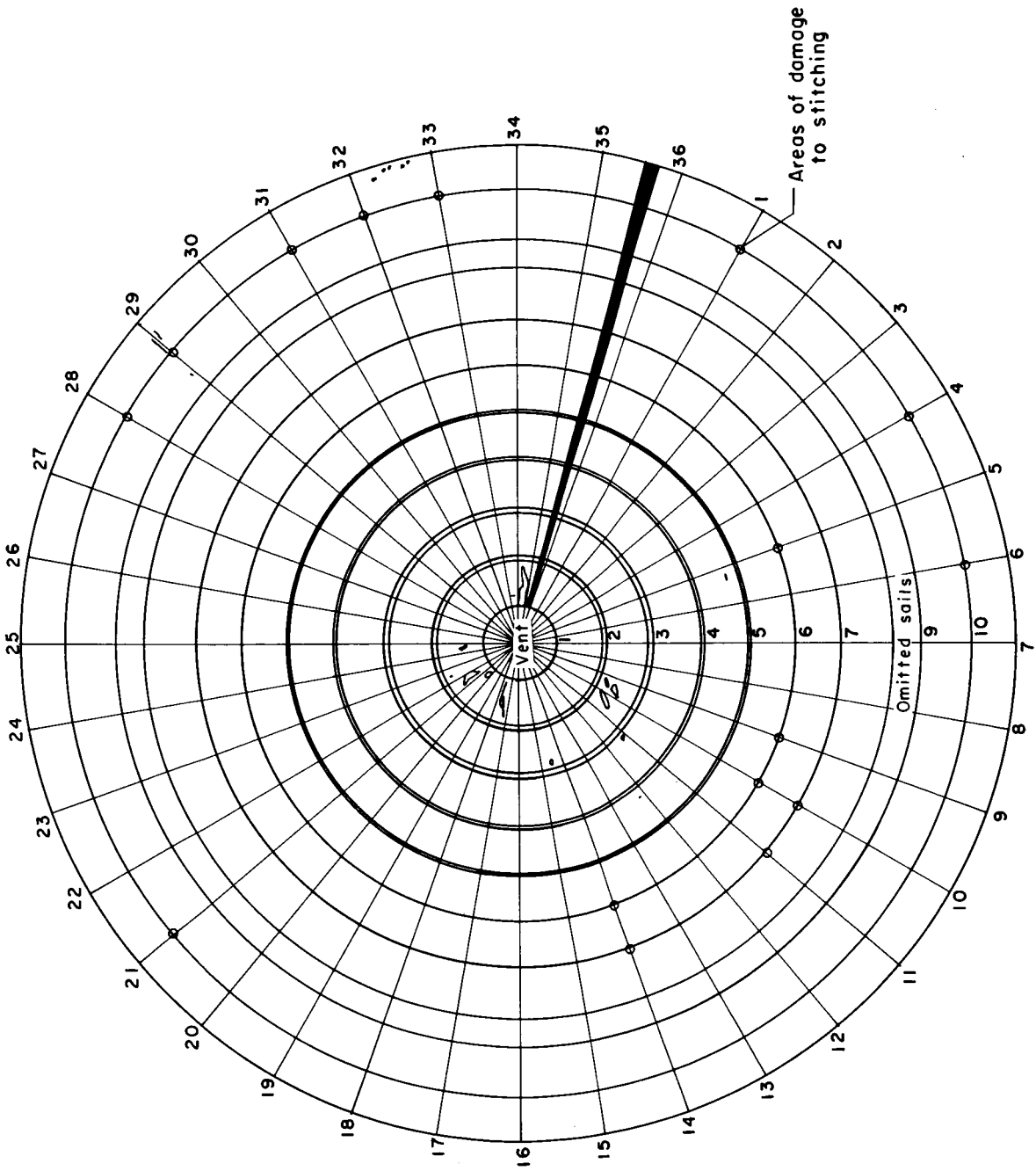
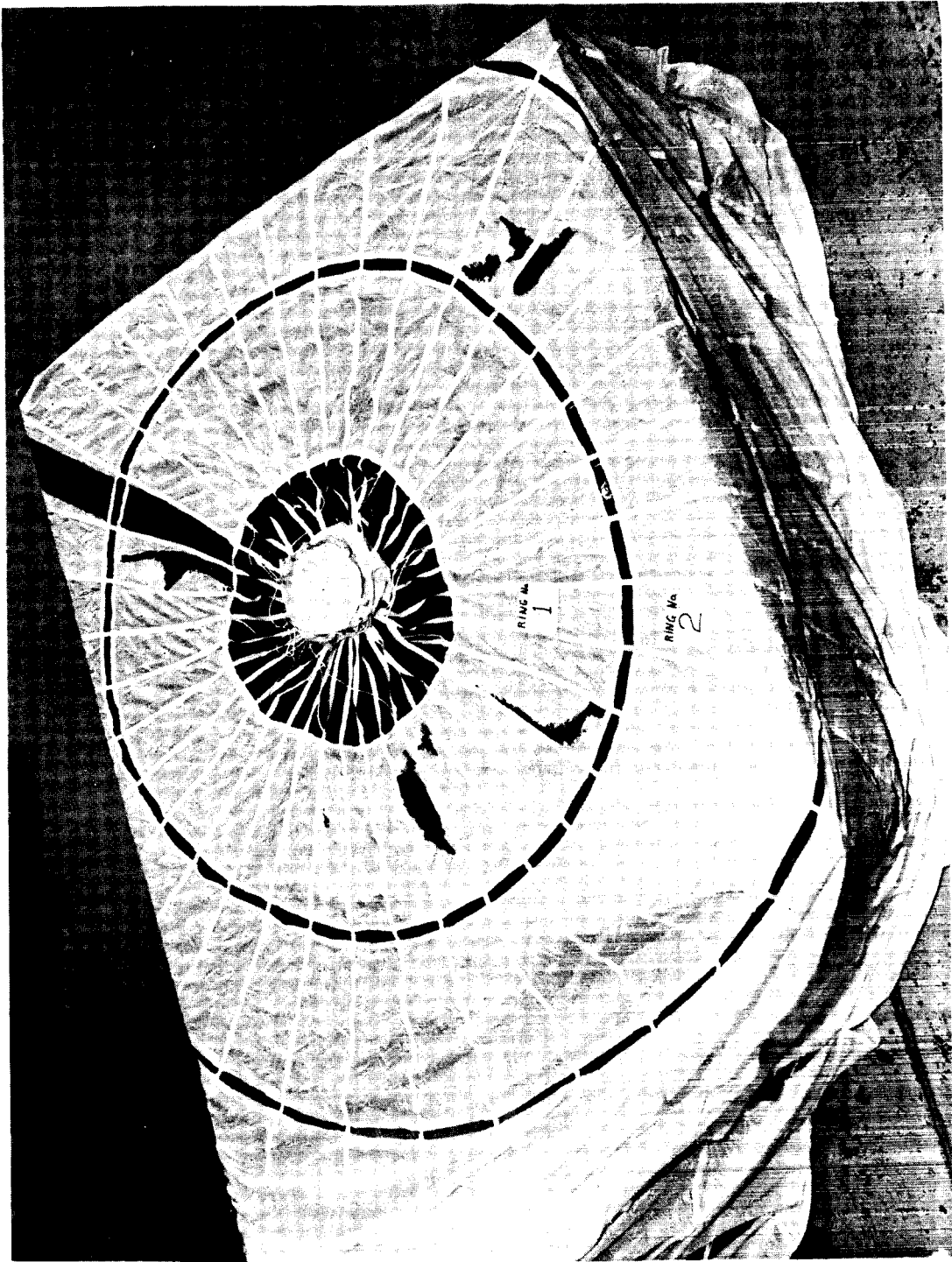


Figure 24.- Schematic showing canopy damage.



L-69-5248

Figure 25.- Photograph showing damage in the vent area of the canopy.



Figure 26.- Photograph of damage in sail 10 at gores 28 and 29.

L-69-5249